SIMPSON, JENNIFER H. Ph.D. The Epitranscriptomic Analysis of Glioblastoma with and without Drug Resistance. (2022)
Directed by Dr. Norman H.L. Chiu. 84 pp.

Glioblastoma (GBM) is the most common, aggressive, and deadly type of malignant brain tumor. Despite the standard of care treatment including maximal surgical resection of the tumor, radiation, and chemotherapy, the median survival rate of GBM patients is only 15 months with a 5-year postdiagnosis survival of 5.8 %. Resistance to chemo or radiotherapy develops with GBM reoccurrence. While much has been uncovered regarding GBM biology in recent years from the mass of multi-omics studies, they have unfortunately failed to translate to clinical success. A new field of study, epitranscriptomics, was created in part by the discovery that RNA modifications have reader, writer, and eraser enzymes indicative of regulatory potentials. These evolutionarily controlled modifications maintain cellular functions and thus overall health. The dysregulation of specific RNA modifications and their associated enzymes in disease states, suggests their importance. However, there are no reports to date regarding the association of specific profiles of RNA modifications in cancer or GBM. In this work, a novel and accurate LC-MS/MS standard-free quantitation of ribonucleosides that allows for 81% coverage of the epitranscriptome of glioblastoma with 96% accuracy is detailed and validated. The modulation of the GBM epitranscriptome to one of temozolomide (TMZ) resistance is delineated in vitro and in vivo. The upregulation of N6-methyl-N6-threonylcarbamoyladenosine (m6t6A) is identified as a target biomarker in GBM resistant to TMZ. Knockdown of the specific writer gene for the RNA modification m6t6A, tRNA methyltransferase O (TRMO), shows promise for resensitization to TMZ treatment in preclinical GBM models. Following RNA isolation, purification, and fractionation, the upregulation of m6t6A is shown to be localized to the tRNA of GBM model LNZ308 with induced resistance to TMZ.

THE EPITRANSCRIPTOMIC ANALYSIS OF GLIOBLASTOMA WITH AND WITHOUT DRUG RESISTANCE

by

Jennifer H. Simpson

A Dissertation

Submitted to

the Faculty of The Graduate School at

The University of North Carolina at Greensboro

in Partial Fulfillment

of the Requirements for the Degree

Doctor of Philosophy

Greensboro

2022

Approved by

Dr. Norman H.L. Chiu
Committee Chair

DEDICATION

To John,

Maker of my lunches, personal encourager, and dad joke king without you I could not have accomplished this. You are my most loyal friend. I will love you forever.

To Fisher, Lily, and Jack,

You have pushed me to be a better version of myself when I didn't always want to be. I want nothing more than for you to truly believe that you can overcome. That you can persevere. That you can do whatever you set your mind to do. And, that you can be happy. Gratefulness is the key. Be kind to each other always. I have faith in the beautiful humans that you have become. My loves, you are everything to me.

To my parents,

You have both endured more throughout this life than most can ever imagine. Even still, I have never doubted your love for me. That is something to be proud of.

To Sandy and Al,

You are an absolute rockstar example of stability and support. There have never been greater cheerleaders to have in your corner.

To Kimberly and Auburn,

We have loved, laughed, and cried through this life together. Crying is for the birds. Let's not do that the second half.

APPROVAL PAGE

This dissertation written by Jennifer H. Simpson has been approved by the following committee of the Faculty of The Graduate School at The University of North Carolina at Greensboro.

Committee Chair

Dr. Norman H.L. Chiu

Committee Members

Dr. Bakhos Tannous

Dr. Qibin Zhang

Dr. Ethan Will Taylor

June 7, 2022

Date of Acceptance by Committee

June 7, 2022

Date of Final Oral Examination

ACKNOWLEDGEMENTS

What a privilege to be a part of a legacy that has supported women in STEM before STEM was a thing. I am forever grateful for this opportunity offered to me by the Department of Chemistry and Biochemistry at UNCG. Thank you for building a community that cares. Within that community, Dr. Daniel Todd, has exemplified what it means to be a mentor. He has patiently answered all 3 million of the questions I have had for him regarding mass spectrometry, analytical chemistry, or the process of earning a PhD. I cannot express my gratitude enough to my dissertation committee, Will Taylor, Qibin Zhang, and Bakhos Tannous for your time and support throughout this process. Bakhos, I am especially grateful for the effort you made to make me the best almost biologist that you could. I wish you all the sunshine that Boston can handle. To my advisor and dissertation chair, Dr. Norman Chiu, thank you for asking me to make a LC-MS method before I even understood what all that entailed. It was probably smart that you didn't explain it to me in detail immediately. I might would have ran. You took a chance on me that changed my life. Thank you for that. This work was funded by the National Institute of Neurological Disorders and Strokes (R21NS118917) at the National Institute of Health, and by the Department of Chemistry and Biochemistry at UNCG. I was also awarded funding for this project through the Dorothy Monroe Family Fund through the College of Arts and Sciences at UNCG and an undergraduate research and creativity award through the URSCO at UNCG.

TABLE OF CONTENTS

LIST OF TABLES

LIST OF FIGURES

CHAPTER I: INTRODUCTION

Glioblastoma

Gliomas comprise 25% of all primary central nervous system (CNS) tumors and 81% of all malignant tumors. Gliomas are classified into grades I – IV based upon histological properties. Grade IV Glioblastoma (GBM), which accounts for a 58% majority of all gliomas, is the most aggressive and deadly form[1,2]. Despite standard of care treatment of maximal surgical resection of the tumor, radiation, and chemotherapy, the median survival rate of patients with GBM is only 15 months with a 5-year postdiagnosis survival of 5.8 %[3,4]. As suggested by cancer progression and mortality found in almost all patients diagnosed with GBM, the effectiveness of the standard of care treatments is limited.

GBM Classifications

Classification of gliomas arose as a means for physicians to predict survival and therapeutic approaches to which tumor heterogeneity poses a major challenge. Tumor heterogeneity can manifest as variability between tumors (intertumoral heterogeneity) or between cells from the same tumor (intratumoral heterogeneity). These differences can be associated with prognostication outcomes or therapeutic responses since each type varies in aggressiveness and treatment resistance. GBM was the first cancer to be genomically and transcriptomically described by The Cancer Genome Atlas (TCGA) initiative which has expanded GBM classifications to include molecular markers as well[5,6]. The studies identified the GBM specific molecular intertumoral heterogeneity and extended GBM classifications to three gene expression subtypes: proneural, classical, and mesenchymal [78]. Proneural is identified by the alteration of platelet-derived growth factor receptor alpha (PDGFRA), cyclin dependent kinase 4 (CDK4) and isocitrate dehydrogenase 1 (IDH1) point mutations. This subtype is typically younger in age with longer survival due to IDH1 mutation[9,10]. Epidermal Growth Factor (EGFR) amplification, the deletion of cyclin dependent kinase inhibitor 2A (CDKN2 A) which is

known to act as a tumor suppressor by regulating the cell cycle, and the lack of tumor protein 53 (TP53) mutations characterize the classical GBM subtype. The more aggressive mesenchymal subtype with its Cr5q deletions and neurofibromatosis type 1 (NF1) alterations is correlated with poor outcome and aggressiveness [8,11–15].

Standard of Care Treatment

The first line of therapy for nonrecurrent GBM includes surgery followed by radiotherapy and administration of temozolomide (TMZ), a DNA alkylating agent. One attractive quality about TMZ is its ability to cross the blood brain barrier (BBB) due to its lipophilicity and small molecular weight [16]. The BBB works to protect the neuronal environment from most blood borne materials which in turn limits therapeutic success for the treatment of GBM. TMZ works by the addition of methyl groups to N-7 or O-6 positions of guanine or N-3 of adenine subsequently inhibiting DNA replication. TMZ is a prodrug that is quickly absorbed and spontaneously hydrolyses to the active form 5-(3-dimethyl-1-triazenyl) imidazole-4-carboxamide (MTIC) that rapidly breaks down to form the methyldiazonium ion, the purine methyl donor [17]. The N-7 methylation of guanine represents 80-85% of total alkylations while the N-3 methylation of adenine makes up 8-18%. Although the O-6 position of guanine accounts for only 8% of TMZ's activity, it provides the most anti-cancer effect [18.] Direct repair of O-6 methylguanosine (O-6 MeG) can occur if the methyl adduct is removed or erased by the suicide enzyme methylguanine-DNA methyltransferase (MGMT) [19]. The unrepaired O-6 MeG does not conform to expected Watson-Crick base pairing and mismatches with thymine instead of cytosine during DNA replication. This alerts another DNA repair mechanism, mismatch repair (MMR), that recognizes the thymine insertion and excises it [20]. However, the O-6 MeG remains resulting in repeated cycles of MMR resulting in excess DNA strand breaks which eventually leads to cell apoptosis via cell cycle arrest at G2/M [21–23]. Limitations to the standard of care treatments is due in part to the intrinsic invasiveness of GBM and the infeasibility of complete surgical eradication.

However, the second step in standard of care treatments, radiotherapy accompanied by TMZ chemotherapy, also fails due to acquired or natural resistance to treatment.

TMZ Resistance

Intratumoral heterogeneity in GBM was recently highlighted by single cell RNA sequencing data that shows transcriptomes specific to GBM subtypes within the same tumor[24]. Not only are all subtypes incorporated into the same tumor, but throughout disease progression GBMs can transition from one subtype to another (**Figure 1**). The proneural subtype exhibits the highest rate of plasticity at 59%[8]. GBM phenotypic plasticity of primary GBMs change by over 60% upon recurrence in response to treatments with the mesenchymal subtype being the most stable primary GBM subtype [7,25]. Mesenchymal transitioning in GBM has been related to resistance to therapeutics [26–30]. Proneural to mesenchymal transition (PMT) is the most common subtype shift that can lead to chemo and radioresistance [31–37]. These shifts can be influenced by the microenvironment of the tumor. Microglia communicate with other glioma cells by releasing membrane bound extracellular vesicles (EVs) that contain active proteins, lipids, and RNA [38,39]. NF-κB/STAT3 signaling induced PMT was recently demonstrated through EVs derived from mesenchymal GSC cells[40]. PMT and endothelial to mesenchymal transition (EMT) in carcinoma cells are comparable and show similar characteristics such as enhanced invasiveness and motility that promotes metastasis and chemoresistance [41–45].

Figure 1. Intratumoral characterization of GBM molecular subtypes. Adaptive mesenchymal transitioning occurs with disease progression and is related to therapeutic resistance.

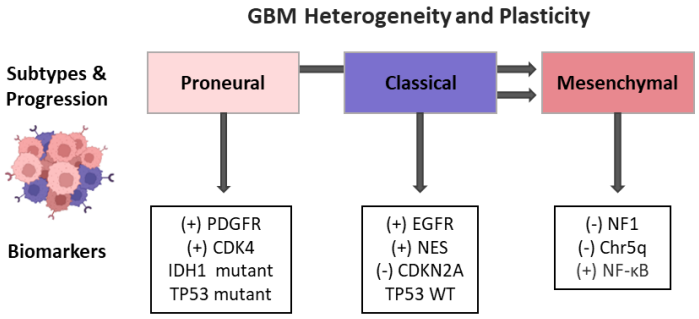

Intratumoral heterogeneity is a main determinant of treatment failure and recurrence due to the divergent cells within a tumor that express variant phenotypic states[46,47].This can be partially explained by the presence of glioma stem like cells (GSCs) which are considered the source of tumor initiation and recurrence since GSCs maintain neural stem-like properties such as self-renewal and differentiation [48,49]. GSCs have the potential to escape chemotherapy induced cell death thus re-entering the cell cycle leading to proliferation and thus mediating tumor resistance[50]. GSCs are also involved in chemoresistance by the activation of DNA repair and multiple response pathways (**Figure 2**)[49,51,52] .

Figure 2. The presence of glioma stem like cells are considered the source of oncogenesis and disease recurrence. GSCs are classified as proneural and mesenchymal with the latter being the more stable form in recurrent GBM tumors. Mesenchymal GSCs are more resistant to radiotherapy with proneural GSCs transitioning to the mesenchymal subtype upon treatment with TMZ. Glycolysis is the only metabolic pathway for proneural GSCs with mesenchymal GSCs utilizing either glycolysis or oxidative phosphorylation depending upon the microenvironment.

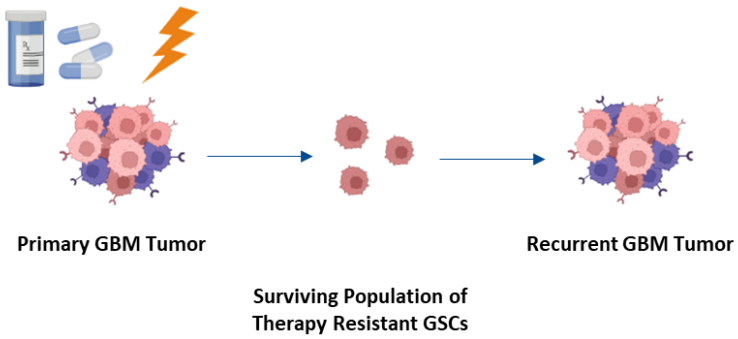

Direct DNA repair by MGMT is the only cellular mechanism capable of repairing the methylated adducts to guanine induced by treatment with TMZ. The overexpression of MGMT by promoter hypomethylation in some GBMs accounts for the 50% response rate in nonrecurrent TMZ treated patients [53,54]. Other indirect DNA repair pathways have also shown to be alternate pathways of chemoresistance in GBM. MMR protein complex mutations can be intrinsic or acquired through treatment with TMZ. By either source, these mutations reduce the

efficacy of TMZ by allowing DNA replication and the cell cycle to continue [55,56]. Base excision repair (BER) is responsible for repairing 90% of TMZ-induced alkylation in the forms of N-7 MeG and N-3 MeA. The first enzyme, *N*-methylpurine-DNA-glycosylase (MPG), in the BER process is highly expressed in TMZ resistant GBM cells [57]. This over expression of MPG leads to the rapid efficiency of the BER pathway that is ultimately responsible for the low cytotoxicity of the TMZ induced alkylation, N-7 MeG and N-3 MeA [58].

Epigenetic alterations of miRNA have also been implicated in chemoresistance [59]. MicroRNA is a single stranded non-coding RNA about 22 nucleotides in length that function in post-transcriptional gene regulation of various oncogenes by mRNA degradation and translational repression [60]. The first known miRNA in GBM attributed to the oncogenic processes of proliferation, apoptosis, and tumor invasion is miRNA-21 (miR-21)[61]. Inhibition of miR-21 was able to resensitize TMZ resistant GBM to treatment in vitro[62]. Another example of a strong oncogenic is miR-10b. Cell cycle and mRNA splicing/alternative splicing are affected by miR-10b in GSC with in vivo and in vitro models. Pre-clinical inhibition studies also concluded that progression of established intracranial GBM reduced with treatment [63]. Sana et al. identified miRNAs specific to GSCs that correlated with survival of GBM patients. This and the substantial number of studies that consider miRNAs in GBM suggests that GBM chemoresistance is directly and/or indirectly controlled by numerous miRNAs. These miRNA correlate with the multiple known pathways of resistance such as the caspase triggered apoptosis pathway in TMZ resistance and miR-21 [64].

Apoptosis and autophagy, key affecters of cell fate, are mechanisms likely involved in TMZ resistance. Apoptosis is a form of programmed cell death. Lower expression ratios of apoptotic proteins Bax/Bcl-2 in GSCs favors apoptosis in recurrent GBM and modulation of pro- and anti-apoptotic proteins imparts TMZ resistance[65,66]. In 2014, preclinical studies of Bcl inhibitors are reported as effective strategies for overcoming apoptosis resistance [67,68]. Autophagy is the conserved degradation of damaged or abnormal proteins, macromolecules,

organelles, or pathogens are delivered to lysosomes and recycled into the cytosol. The induction or inhibition of autophagy can be initiated as a cellular stress response leading to cell death or survival. TMZ has induced a cytoprotective autophagy ATP surge in GBM cells in a potential contribution to drug resistance [69].

The BBB functions as a protective barrier against toxins or pathogens that selectively allows nutrients to not only reach the brain, but it also maintains the brain in homeostatic balance. The BBB is composed of endothelial cells that line the brain microvascular and create tight junctions between the cells. These tight gaps permit transcellular passive diffusion of small, lipophilic compounds while other compounds must cross by transporter-mediated active transport. There are numerous membrane-bound transporters responsible for the influx or efflux of substrates into and out of the brain [70,71]. This evolutionary conserved protection mechanism is one of the major challenges in neuro-oncology. In GBM, efflux pumps are significantly upregulated acting as a resistance mechanism for known and new chemotherapeutics [72,73]. While GBM has also been shown to physically disrupt the integrity of the BBB it has not translated to improved drug delivery efficacy[74,75].

The Epitranscriptome

At the cellular level, depending on the cell type and its status, our genome is selectively transcribed into a set of unique ribonucleic acid (RNA) molecules (or transcriptome). Besides playing a central role in the process of protein synthesis, RNAs are directly involved in other cellular activities at both genomic and proteomic level, such as maintaining the integrity of telomeres and the post-transcriptional regulation of gene expression.

To support all RNA-dependent cellular activities including protein synthesis with adequate specificity and effectiveness, a unique and specific transcriptome is required. Despite the transcriptome being made up of different types of RNA molecules, which may vary in size and/or RNA sequence, the diversity of a transcriptome is limited by having only four basic building blocks, namely adenosine, uridine, guanosine, and cytidine. Through the advances in

technology and methodology for measuring the subtle changes in RNA biomarkers, we now have realized that the structural diversity of a transcriptome is significantly enhanced by RNA modifications. RNA modifications are decorations on the chemical structure of the four canonical RNA bases, sugar, or even the phosphate group that makes up the monomeric units of RNA known as a ribonucleotide (**Figure 3**). In 1956, Davis and Allen discovered the first RNA

Figure 3. While RNA modifications are not limited to methylations the above example also highlights structural positioning of modifications on adenosine.

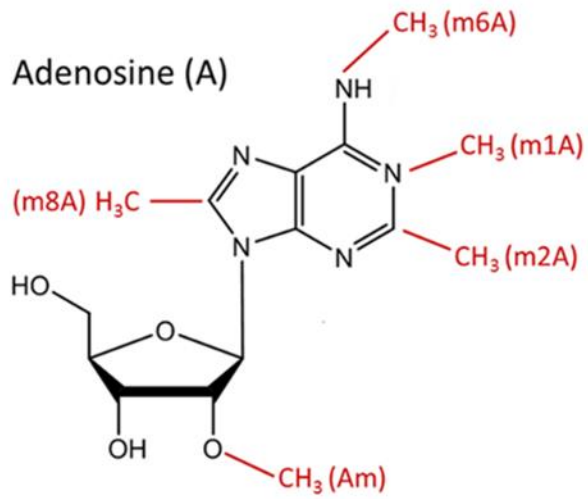

An Example of Adenosine Methylation

modification known as pseudouridine which is an enzymatic isomerization of uridine that leads to an additional hydrogen bond and a unique carbon-carbon glycosidic bond [76]. Since that time, over 150 of these distinct modifications have been identified [77]. Methylation is the most abundant class of RNA modification and can be found at different positions of the heterocyclic bases of the canonical ribonucleotides and on ribose moieties [78]. Adenosine to inosine editing (A-to-I) is a special category that results from enzymatic deamination of adenosine creating the non-canonical inosine. Inosine translates as guanosine altering translation and transcriptional processes[79]. Other RNA modifications can require complex multistep or multi-enzymatic synthesis for simple O to S exchange or the addition of bulky substituents such as amino acid residues, sugars, or fatty acids.

RNA Modifying Proteins

The central dogma of molecular biology describes the flow of genetic information from DNA that is copied to RNA which provides the formula of proteins (**Figure 4**). The discovery of modifications to nucleic acids expanded the complexity on the regulations between DNA and proteins. A new field of study, epitranscriptomics, was created in part by dynamic effector enzymes involving m^{6}A (*N*^{6}-methyladenosine). m^{6}A is the most abundant internal modification in mRNA (0.1 – 0.4%) which accounts for 3 to 5 m^{6}A modifications per mRNA molecule [80]. In 2011 the He group was the first to report that m^{6}A could be demethylated by the demethylase FTO [81]. FTO has since been shown to preferentially select for m^{6}Am (*N*^{6},2′-*O*-dimethyladenosine) with ALKBH5 being the primary demethylase for m^{6}A but the impact suggesting that m^{6}A could be dynamically regulated along with two m^{6}A mapping studies brought renewed interest to the field [82,83]. RNA modifying proteins (RMPs) have been coined as writers, readers, and erasers based on epigenetic terminology for enzymes or proteins that add, remove, or preferentially bind to the chemical modifications of RNA nucleotides [84]. Some RMPs can promiscuously modulate multiple RNA species or even RNA modifications, while others exclusively affect specific RNA species or modifications. Since the characterizations of FTO and ALKBH5, the number of

Figure 4. The central dogma of molecular biology respective to the epitranscriptome.

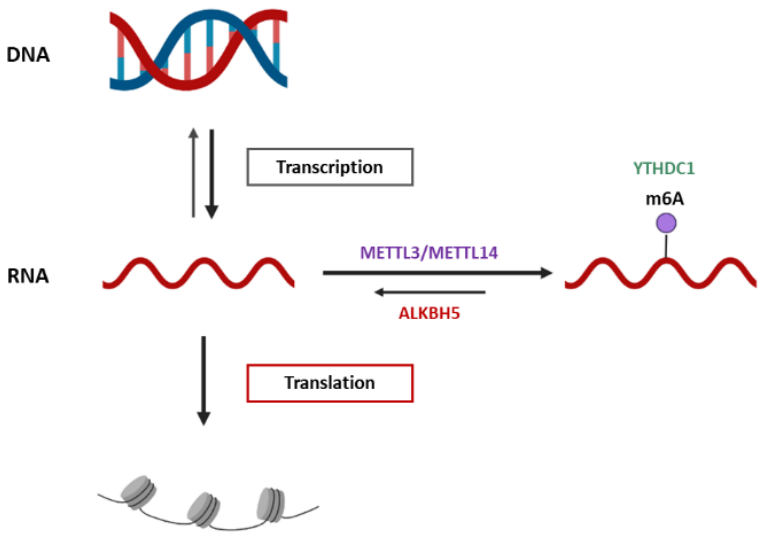

erasers identified are small when compared to the number of writers and readers identified. Thus, new arguments have been made regarding the dynamics of RNA modifications as driven by writers as the more efficient mechanism of regulation in part due to the short half-lives of transcripts [85–87] .

Dysregulation of the Epitranscriptome in GBM

Modifications to RNA not only changes the structure of an individual nucleotide but can also influence the biological function of the RNA molecule by affecting secondary or tertiary structures. Folding patterns in RNA are necessary for maintaining functional structures. As such, RNA modifications are a classic representation of the structure function relationship in biochemistry. Our collaboration with the Tannous group reported that most RNA modifications with a single modification do not interfere with RNA duplex formation. However, there are modifications, like inosine, with destabilization potential by decreased hydrophobicity. Also, modifiers position inside or outside the helical structure impact the stability of transcripts and thus translational fidelity as well as RNA binding protein (RBP) recognition [88]. Essentially, post-transcriptional modifications expand RNA vocabulary facilitating molecular recognition in coding and noncoding RNAs. Examples are seen in the anti-codon sequence of tRNA[89], rRNA structure enhanced translation and biogenesis[90], and gene expression regulatory control through mRNA[91] and miRNA[92] .Evolutionarily controlled RNA modifications require a significant energy cost to maintain cellular functions and overall health, suggesting their importance. Conversely, disruptions or alterations in RNA modifications and RMPs have been found to occur in disease states including human cancers [93–95].The implications of RNA modifications specifically related to GBM remain largely unexplored. To date most studies have been relegated to the RNA modifications and corresponding RMPs identified in mRNA for m6A, m6Am (N^6, 2′O-

Figure 5. Known mRNA modifications with chemical structure and known reader, writer, and eraser enzymes.

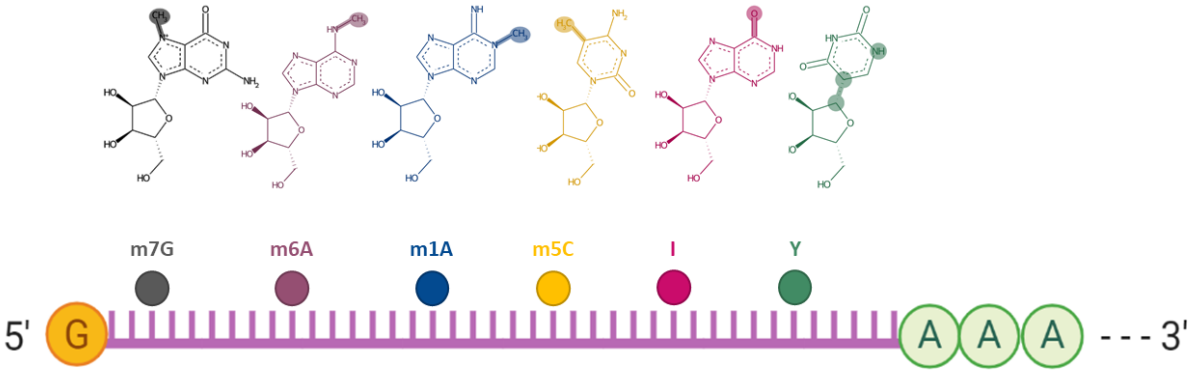

METTL1 WDR4 RNMT	METTL3 METTL14 WTAP	TRMT6 TRMT10C TRMT61A-B	NSUN1-5 DNMT2	ADAR1-3 ADAT1-3	PUS1-10 PUS7L RPUSD1-4 DKC1	Writers
unknown	YTHDF1-3 YTHDC1-2	YTHDF1-3 YTHDC1	ALYREF	unknown	unknown	Readers
unknown	ALKBH5	ALKBH1&3	unknown	none	unknown	Erasers

dimethyladenosine), m1A (N^1-methyladenosine), m5C (5-methylcytosine), I (inosine), 7-methylguanosine (m7G), and Y (pseudouridine) (**Figure 5**).

Inconsistent findings have plagued the most studied RNA modification, m6A. Writers for m6A, methyltransferase-like 3 (METTL 3) and methyltransferase-like 14 (METTL14) have been contradictorily related to GSC stem like properties of tumorigenesis, proliferation, self-renewal, and migration. Inverse expressions have also been connected to apoptosis, radiosensitivity and state of malignancy[96–98]. Other studies have included the demethylase or eraser, FTO, the now accepted primary demethylase of m6Am which raises the question if m6Am is the responsible modification rather than the accredited m6A. Another factor for inconsistency could arise from the failure or inability to validate GBM intra or intertumoral heterogeneity as seen when one report used glioma tissue samples without disclosure of the grade [99]. However, corroborated studies describe an elevated WTAP expression increases EGFR expression, a known amplified clinical biomarker of GBM[100–103]. WTAP (Wilms' tumor 1-associating protein) is associated with

the m6A writer complex and plays an essential role in regulating the activity towards mRNA targets [104,105]. Overexpression of the decided primary eraser for m6A, α-Ketoglutarate-dependent dioxygenase alkB homolog 5 (ALKBH5), facilitates proliferation and tumorigenesis of GSCs with poor patient survival through FOXM1. In support, knockdowns of ALKBH5 and the antisense FOXM1 (FOXM1-AS) disrupted GSC tumorigenesis [106]. A group of YTH domain-containing proteins have been characterized as m6A readers. An elevated expression of Insulin like growth factor 2 mRNA binding protein 1-3 (IGF2BP1/IMP1-3), one of several identified m6A readers, has been implicated in EMT and chemoresistance [107]. Zhu et al. reports that an oncopeptide regulates m6A recognition by IGF2BP1 promoting tumorigenesis [108]. As the most studied modified RNA there are more exhaustive reviews of the regulatory role of m6A in cancers and glioblastoma [37,109–113].

Beyond m6A six more of the 150 known RNA modifications or RMPs were identified in GBM studies (m7G, m6Am, m1A, m5C, Y, and I). Methyltransferase 1 (METTL1) is the writer for m7G in tRNAs. The overexpression of METTL1 induces oncogenicity with poor patient survival in a codon biased manner that acts upon the tRNA Arg-TCT-4-1 [114]. Besides the potentially misappropriated studies for FTO, the primary eraser of m6Am, the m6Am reader decapping mRNA 2 (DCP2) has also been associated with glioblastoma. DPC2 is upregulated with the overexpression of miR-338-5p leading to radiosensitivity and DNA damage response[115]. It has also been shown as a top 20 hub gene target for competing endogenous RNAs (ceRNA) in glioblastoma suggesting the potential role of m6Am in the development of GBM[116]. The substrate binding unit tRNA methyltransferase 6 (TRMT6) is a known writer for m1A whose dysregulation has been correlated to poor clinical outcome in cancer [117–119].

Genomic aberration of NSUN5, a DNA m5C methyltransferase, has been extensively discussed once highlighted by TCGA [120]. Since that time, the RNA modification m5C has been identified in most RNA species with writers found in the NOL1/NOL2/sun domain RNA methyltransferase family. The writer used is dependent upon RNA species. This expression

profiles of the m5C methyltransferase family of enzymes have been recently used to predict malignancy and prognosis in GBM[121]. In RNA, NSUN5 downregulation in 28S rRNA restrains overall protein synthesis and promotes activation of mRNA translational program for stress survival. Molecular modeling confirmed m5C at C3782 of 28S rRNA acts to stabilize the tertiary rRNA-mRNA-tRNA structure [122,123]. NSUN2, another m5C writer, is a target gene of nuclear respiratory factor 1 (NRF1). High expression of both leads to poor survival and TMZ resistance possibly through NFR1 regulated PMT which makes NSUN2 a potential combinatorial therapy [124]. NSUN6 is a promiscuous writer for m5C described to control response to TMZ via NELFB and RPS6BK2 [125]. The m5C mRNA reader linked to NSUN2, Aly/ REF export factor (ALYREF), drives proliferation in glioblastoma by an ALYREF-MYC positive feedback loop[126]. With the outpouring of new work implicating RNA m5C in cancer and glioblastoma an updated review would be of great value to the field.

Pseudouridine is the most frequent cellular RNA modification with biological functions including rRNA folding, tRNA codon/anti-codon pairing, and mRNA secondary structure enhancement altering binding of RBPs[127]. Recently, Cui et al. observed that the overexpression of PUS7, a writer for Y, in GSCs regulates tumorigenesis and is associated with poor patient prognosis through codon bias translation controls [128]. Targeting PUS7, a RMP specific to Y, suppressed tumor progression in mice representing preclinical significance as a potential drug target [129]. Wang and coworkers constructed a glioma prognosticator model that implicated the TME with the pseudouridine writers PUS7, PUS1, RPUSD1, DKC1 and TRUB1[130].

Inosine in the wobble position of tRNA expands translation by writing C, A, and U ended codons. It also can base pair with guanosine in mRNA influencing interactions with RBPs by altering duplexes, affecting splicing and translational fidelity[131]. In gliomas, overexpressed writers ADAR 1 and 2 contribute to GBM oncogenesis[132]. In miRNA dysregulation of miR-376a-39 by ADAR attenuation promotes invasiveness of GBM cells[133]. A combinatorial relationship between inosine and m6A occurs by overexpression of ADAR1 by METTL3 (m6A writer) and

YTHDF1 (m6A reader) promoting GBM proliferation by CDK2 stabilization via ADAR1[134]. This year another novel combinatorial relationship was exposed by Xu et al. elucidating EMT transition associated with the TME and the NF-κB pathway by two distinct RNA RMPs involving C to U editing through UPP1 and FTO, the eraser of m6Am and m1A. The 6 non-m6A modifications above were shown to be prognosticators of GBM subtype and diagnostic modeling highlighting their therapeutic value[135].

Next Generation Sequencing

It is well established that RNA modifications are variably present on most RNA species. Providing single nucleotide resolution sequence context for a specific modification across differing RNA species is not only essential it is the primary advantage of NGS. The transcriptional location of RNA modifications is necessary for ascertaining mechanisms of action and biological relevance[136]. Unfortunately, with NGS this comes at the expense of other epitranscriptomic modifications which have newly confirmed combinatorial regulatory potential as discussed earlier. Another weakness of NGS is the indirect detection of epitranscriptomic marks[137]. NGS sensitivity is based upon the ability to amplify RNA signal by RNA dependent RNA polymerase reverse transcriptase (RT). During primer extension or amplification RNA transcripts are converted to an inverse copy known as cDNA. Modifications are lost in the RT process and can show as an abortive stop in the cDNA, as commonly seen with bulky modifications. Other modifications may lead to the incorporation of a non-complimentary canonical ribonucleotide while some RT silent epitranscriptomic marks, like m5C, do not affect expected Watson Crick pairs leaving an unmodified template. Thus, the majority of NGS approaches are built to selectively enhance RT stops for the indirect detection of modifications[138]. This occurs by taking advantage of naturally existing RT signatures, chemically induced RT stops, chemically induced cleavage of the ribose-phosphate backbone and selective ligation, and antibody enrichment methods[139]. In theory, selective RT stops increases accuracy and sensitivity as seen with confidence in m6A, I, and Y. This is, however, not always

the case. With the drive for new approaches that expand mapping beyond m6A, highly divergent m1A mapping forced the field to publish multiple reviews and commentaries discussing sources of error in NGS approaches and establishing quality metrics for new maps[140–144]. The controversial m1A mapping was later attributed to antibody selectivity when Grozhik and coworkers identified cross reactivity between the two positively charged purines m1A and m7G[145]. This finding challenged antibody specificity in the field raising the question if a single methyl group could provide sufficient selectivity for mapping lower abundant modifications since there will also be binding affinity for all derivatives of the nucleobase at varying degrees[146]. While m1A may have instigated the conversation it was not the only problematic NGS mapping implicated. Low accuracy localization with bisulfite treatment occurs since the treatment protects cytidine derivatives from the deamination seen in unmodified cytidine that generates uridine following a Michael's addition reaction[147]. Careful validation of future work is fundamental for the integrity of the field [140] .

Nanopore Sequencing

Unlike NGS sequencing, third generation nanopore sequencing directly sequences single long native RNA molecules (~20kb). Flow cells contain nanoscale protein pores, or nanopores, that are embedded into an electro-resistant polymer. Each nanopore acts as an individual biosensor that measures the electric current that flows through it. This current is produced in an electrolytic solution when a constant voltage is applied. Taking advantage of the intrinsic negative charge on RNA, it is pushed from the negatively charged cis side of the nanopore to the positively charged trans side. As RNA molecules pass through the nanopores, changes or disruptions in the ionic current correspond to specific ribonucleosides and are decoded using algorithms for direct real time sequencing [148–150]. This technology could eventually be a game changer for RNA and DNA sequencing[151]. It provides direct long read sequences at lower cost with the simultaneous detection of base modifications with no pre-processing treatments. However, with its reliance on algorithms the diversity of

epitranscriptomic marks and need for large amounts of sample can be troublesome for assignments. Currently base calling errors range from 10-15% without single nucleotide resolution. Limited analytical standards for RNA modifications are a major challenge for any epitranscriptomic technology and are required for algorithm training to be able make assignments with nanopore sequencing[152–155]. Lastly, some modifications with large chemical groups may completely block the nanopore [156]. Nanopore sequencing, while still in its early stage of development, holds high potential for epitranscriptomic analysis.

Mass Spectrometry

Mass spectrometry used in tandem with liquid chromatography (LC-MS/MS) gives high accuracy identification, robust quantitation, and is currently the only technique that can simultaneously identify upwards of 25 ribonucleosides at once[157]. With the dynamic and combinatorial nature of the epitranscriptome at potentially low abundance, mass spectrometry is an ideal platform choice.

With LC-MS/MS the mixture of RNA is first introduced to a metered flow of solvent or mobile phase that flows through a pressurized column packed with a separation medium or stationary phase. Migration of separated RNA is driven by the composition of the mobile phase and chemical interactions with the stationary phase. As the separated RNA emerges from the column it flows to the mass spectrometer for detection. First, the sample is converted from a liquid to an ionized gas phase which is further separated based upon each ion's mass to charge ratio (m/z) and detected in proportion to abundance. Low resolution/high sensitivity instruments like triple quadrupoles (QqQ) can detect attomole to femtomolar concentrations increasing the quantitative global epitranscriptomic coverage independent of sample type but with targets selected *a priori*. Whereas high resolution/low sensitivity instruments like time-of-flight (TOF) or orbitraps are highly accurate and selective allowing for untargeted screening with fragmentation increasing confidence in structural determinations. Experimental design is the determinant of

which mass detector to be used. Overall, there are 3 types of MS based analysis of RNA with each requiring a different level of enzymatic preparation beforehand.

Top-down MS of non-hydrolyzed RNA maintains sequence context for total mass analysis of RNA including modifications while revealing sample heterogeneity[158–161]. High resolution MS can predict sequences based on their high accuracy and ability to determine charge states. Top-down MS can also be used to investigate RNA-protein complexes and RNA writers and erasers in vitro [162–164]. Current limitations include maximum read lengths of ~60nt with indistinguishable isobaric modifications. Further, spectral data is complex coupled with extremely limited bioinformatic software for processing data makes top-down sequencing by MS tedious and slow.

The more employed bottom-up approach utilizes base specific ribonucleases (RNases) to digest larger RNA into oligonucleotides with chromatographic separation to reduce the mixture complexity of the oligonucleotides. This unbiased approach is commonly called oligonucleotide MS-MS (ON-MS) and can identify multiple modifications in a sequence. The hydrophilic nature conferred by the negatively charged phosphate backbone has created challenges for retention, ionization, and sequencing that has been addressed by ion-pairing reagent chromatography in negative ionization mode, ion-pairing reagent free in negative or ion-pairing chromatography in positive mode[165–167]. Works by McLuckey and Schürch have detailed the predictable fragmentation patterns of intact oligonucleotides after applying energy in the gas phase which allows for modification identification by unique mass shifts [168–170]. In recent years, software and bioinformatic resources have been developed for interpretation and LC-MS/MS mapping like established proteomic sequencing software[171–178].

Nucleoside MS enzymatically digests RNA to its monomer units or nucleosides using endo and exonucleases and phosphatases[179]. Pure samples are required for quantitation of individual species requiring an extra quality control step of chip electrophoresis. The mixture is typically ran with LC-MS/MS or LC-UV-MS/MS. New advances in stationary phases have

improved retention and resolution. Nanoflow liquid chromatography mass spectrometry (nLC-MS) can improve sensitivity thus allowing for a decrease in sample mass[180]. A clever workaround for the limited analytical standards plaguing the field was established by biosynthetic production of stable isotope labeled internal standards (SILIS)[181,182]. However, this approach does not result in a comprehensive set of modifications since different samples contain different modifications and they cannot provide pure modified ribonucleosides individually.

There are limitations that require the attention of the field. A simple yet challenging obstacle lies in the samples themselves. Cellular RNA consists of rRNA (~80%), tRNA (~15%), and mRNA (~5%) not including even lower abundant species like miRNA and circular RNAs. Total RNA is difficult to fractionate into pure individual species and with the mass of sample needed for analysis. Mass spectrometers are sensitive enough to identify and quantify low abundant modifications. This was highlighted in a recent mRNA study that used mRNA enrichment by poly A capture with high salt concentrations which promoted hybridization by other RNA species[183,184]. This contamination erroneously depleted the expected modifications in the sample[185]. Other MS based constraints are the need for increased instrumentation sensitivity and methodologies that create more high throughput sample analysis to compete with other sequencing techniques. Sample labeling for quantitation in manners as seen with iTRAQ in proteomic studies could also address the lack of available standards and lessen the mass of samples needed per injection. More technology-based improvements to MS data banks for spectral searching or matching and mapping would also benefit the field.

Conclusion

Following the standard of care treatment, GBM will reoccur and develop resistance to treatment. The research on resistance mechanisms of GBM discussed here is not exhaustive. The density of cross-discipline studies by teams of scientists trying to address the mechanistic question of how resistance occurs or the therapeutic question of how to treat it demonstrates

just how urgent the clinical need is for patients diagnosed with GBM. Considering the numerous resistance pathways discussed, evidence suggests that resistance mechanisms coupled with the insulation that occurs from the BBB and incomplete surgical resection leads to treatment failure. It is an unfortunate truth that the vast amount of multi-omics data represented has failed to translate to clinical success. However, that same data does address some important considerations for future studies. Mesenchymal subtypes are shown to be the most aggressive and lethal in preclinical and clinical studies. Subtype plasticity studies indicate the proneural shift to mesenchymal correlates with therapeutic resistance. Resistance is often acquired with the inhibition of one target due to cancer specific salvage mechanisms. Combinatorial therapeutic approaches should be further explored for persistent remission. Targeted therapeutics that address the importance of subtype plasticity and transitions could exploit the reversibility of GBM subtypes as a means of resensitization to TMZ.

Recent technological advancement in characterizing and quantifying the epitranscriptome via NGS and LC-MS/MS approaches have broadly expanded the biological relevance these post-transcriptional marks and their associated RMPs have on health and disease. There is evidence of cancer progression by RNA modifications modulating mesenchymal GSC properties of proliferation, differentiation, migration, and drug resistance [186–188]. The limited studies delineating the regulatory control of the epitranscriptome in GBM are mostly focused on the 7 of 150 known modifications that have been identified in mRNA although it is well established that other species of RNA have regulatory capacity. Focusing on specific RMPs for knockdown and/or overexpression will help elucidate their biological relevance and probability as drug targets. Some RMPs are promiscuous meaning that they either act on one modification across different RNA species or they act on multiple modifications across one or more species of RNA. Others are selective to a specific modification on a specific RNA species which makes them interesting for pharmacological studies. The very structural nature of RMPs as containing well-defined binding pockets suggests their potential for inhibition or modulation in

precision cancer therapeutics but requires the direct experimental testing of each target. This is especially attractive for GBM studies because the people who are diagnosed are desperate for more time. Another relevant question is, if the different grades of gliomas can be phenotypically subtyped does it persist to their global epitranscriptomic profiles? Could this help with diagnostics or mechanistic leads? The idea of phenotypic global epitranscriptomes has yet to be explored since most attention has been placed on singular and select RNA modifications (**Figure 6**).

Figure 6. The epitranscriptome as diagnostic biomarkers or druggable targets for GBM with and without drug resistance as elucidated by LC-MS/MS.

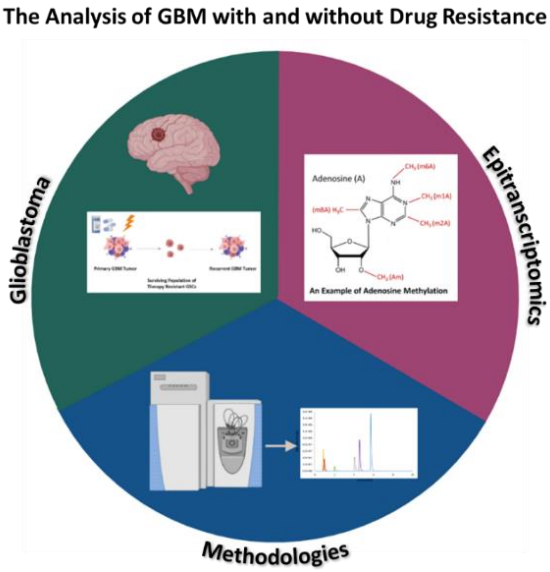

CHAPTER II: PROJECT METHODOLOGIES AND VALIDATIONS

Introduction

The global epitranscriptome of GBM with or without drug resistance has not been reported to date. To facilitate this a qualitative and quantitative method capable of detecting a mixture of ribonucleosides with abundance covering upwards of 4 orders of magnitude as found in biological assays was required. As the only approach capable of the simultaneous detection of RNA modifications and with a group precedence LC-MS/MS was the chosen approach to answer the first questions of can we do this? Followed by is there a difference in the GBM epitranscriptomes with and without drug resistance? Answering the second part of that required the collaborative efforts with the laboratory of Prof. Bakhos Tannous at Massachusetts General Hospital, who has dedicated his entire career to the study of GBM.

During our initial studies, we identified several limitations with some of the LC-MS/MS methods found in literature. First, the chromatographic separations were not always optimized for maximum resolution. Instead, the complexity of the mixtures relied upon the resolving power of the MS. This is not technically wrong for targeted MS analysis that has a continuous flow of ions like QqQs. However, when utilizing a high-resolution MS, such as an orbitrap, it is imperative to account for the limited trap space with co-eluting ions that may have orders of magnitude differences in ion density. Other related chromatographic issues to address involved retention time, solubility, and conversion of HPLC to UPLC methods. Converting from HPLC to UPLC was challenging because of poor retention of polar pyrimidine molecules on reversed phase C18 columns. As a potential solution to increase retention hydrophilic interaction chromatography (HILIC) was evaluated. While resolution, retention, and peak shape was attainable with a Waters Acquity BEH Amide column the high organic starting conditions of the mobile phase created solubility issues with some of the ribonucleosides resulting in back pressure issues with the column.

A Waters Acquity polar end capped HSS T3 column was the final solution. Optimization of mobile phase, pH, flow rate, and column temperature followed. Two things to note from validation experiments both pertain to pH. First, many LC-MS/MS approaches use 0.1% v/v formic acid to facilitate ionization by providing protons for positive mode acquisitions. While this is replicated in nucleoside LC-MS/MS, we identified increased depurination at that volume and pH. Depurination was resolved by reducing the formic acid to 0.01% v/v. Secondly, fluctuations in pH significantly effect retention times with the HSS T3 column. The manufacturer recommends storing columns in neat solvents when not in use to prolong the life of the column. This translated to three hours of equilibration time to stabilize retention shifts. It is also recommended to use volumetrics for preparing mobile phase since small changes in pH result in retention shifts.

Reported MS methods mostly involved targeted acquisitions, as seen with low resolution high sensitivity mass spectrometers like QqQs. These methods relied on the neutral loss of 132 m/z for the ribose or 146 m/z for a methylated ribose since the N-glycosidic bond between the nitrogenous base and sugar moiety tends to be the easiest bond to break. In such a case, a one transition identification accompanying a pure analytical standard is satisfactory. However, reliance on a singular neutral loss fragment for untargeted profiling is not sufficient when there is limited ribonucleoside analytical standards available for purchase coupled with the isomeric redundancy found in 61 of 170 known ribonucleosides. To address these concerns, elemental composition was predicted from high mass accuracy. A two-step higher-energy collisional dissociation (HCD) with optimized energy settings enriched fragmentation data which was subsequently compared against MS data banks and in silico fragmentation software to characterize 40 modified RNAs in immortalized GBM models LNZ-308 and U87. It is important to note that the number and identity of modified ribonucleosides are sample based and limited by the sensitivity of the detector. No online or commercial program for epitranscriptomic analysis and no established epitranscriptomic data sets for evaluation are available for data

processing. Therefore, characterization coupled with a robust intralab validated chromatographic separation enabled the creation of an inhouse processing library for reproducibly defining peak areas.

A workflow of the full assay includes isolation and purification of total RNA from 18 nucleotides (nt) to 200 nt bases with purity assessments and an enzymatic digestion of the total RNA to its monomeric units at physiological pH and temperature before HRMS-MS analysis (**Figure 7**). To account for low abundant modifications 500 ng of relatively pure RNA is needed

Figure 7. Complete epitranscriptomic LC-MS/MS workflow.

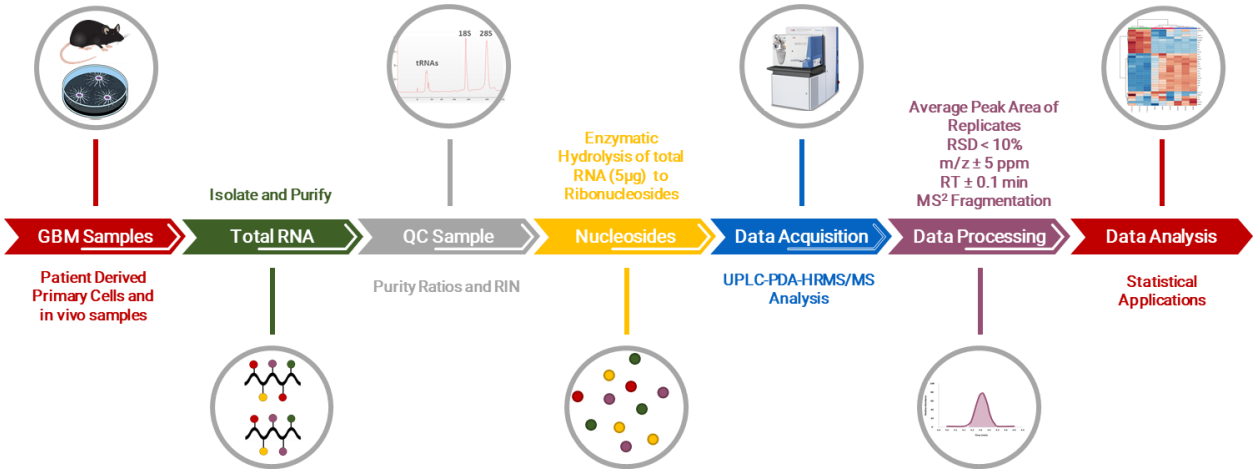

for each LC-MS/MS experiment. RNA extractions are fairly routine with many commercial kits available on the market for purchase. Care must be taken to assure that the appropriate extraction technique is used to maximize purity and yield of preferred RNA. RNA yield differs by sample type. Kits that utilize silica-based microcentrifuge spin columns have a mass capacity. Attention to manufacturer's specifications is important to avoid oversaturation of the column which can lead to preferential binding. Also, RNA species are made up of specific nucleotide base lengths and not all extraction methods yield the full range of RNA species. The use of isopropanol to precipitate RNA is biased towards small RNAs and can cause poor resolubilization affecting downstream purification and analysis of RNA[189]. Phenol-chloroform

extractions that partition DNA from RNA is dependent on pH[190]. A decrease in pH by acidic phenol (~pH 4.8) isolates RNA in the aqueous phase and DNA in the interphase or organic phase[191].

Purification assessments of total RNA require a 260/280 UV based ratio of ~ 2.0. A reduced 260/280 ratio may indicate the presence of protein or phenols that can absorb light at 280 nm wavelength. A secondary 260/230 purity ratio of ~2.1 is expected for RNA. Contamination by salts, carbohydrates, peptides, and phenol can lower this ratio. If contamination from alcohols or phenols occur this can potentially inhibit downstream enzymatic hydrolysis of RNA. However, there is no consensus on how low is too low for this ratio partly because that would be contaminant dependent. Further, spectrophotometric absorbance-based readings cannot detect RNA degradation. Chip based electrophoresis is a means of quality control necessary to assure the integrity and comparability of RNA samples. Failure to examine the integrity of the RNA will impair quantitative measures by diluting the RNA and thus modifications present or by introducing unexpected modifications to the analysis. With microfluidic chip-based electrophoresis the ratio of 28S to 18S rRNA in a sample is the determinant of sample degradation resulting in an RNA integrity number (RIN). A perfect RIN is a 28S/18S ratio of 10 with scores of > 8 required for NGS. Chip based electrophoretograms are considered the preferred quantitation method of total RNA due to the use of fluorescent tags that preferentially bind to RNA. Recent advances include newer chip assays for the separation of smaller RNAs (<200nt). In that way both chip assays (~2 pg/µL) can determine the integrity of the sample, more accurate concentration, and purity determinations of fractionated RNA species.

Enzymatic hydrolysis is achieved by a mixture of endo and exonucleases with phosphatase to reduce the polymer RNA to its monomeric form. The original hydrolysis by Crain and collaborators introduces a pH shift (pH 5 to 8) to dephosphorylate ribonucleotides released during alkaline hydrolysis. The more acidic conditions effect the nucleophilicity of the unmodified

2'-hydroxyl group which can in turn decrease stability of certain modifications. This induces artifacts and is not sufficient to remove m7G from the mRNA cap [192–194]. A single step hydrolysis near biological pH helps to ensure the structural stability of some RNA modifications [195].

Cell Culturing

Human GBM cell lines LNZ308 and U87 were cultured in DMEM (with 4.5 g/L glucose and 584 mg/L L-glutamine and without sodium pyruvate) medium supplemented with 10% (v/v) fetal bovine serum and 1% (v/v) penicillin/streptomycin. Patient-derived GBM cells from tumor specimens MGG6, GBM8 (provided by Dr. Hiroaki Wakimoto) and PN157 (provided by Ichiro Nakano) were cultured from discarded tissues under approval of the institutional review board and were previously characterized[196,197]. These cells were grown as spheres in DMEM/F12 medium supplemented with 2% (v/v) B-27 without vitamin A, 3 mM GlutaMAX^{TM}, EGF (20 ng/mL) and FGF (10 ng/mL). Cell cultures were incubated at 37 ^{o}C in humidified conditions equilibrated with 5% CO_2 (g).

Cells were harvested when they reached confluency in a 100 mm dish and transferred to a 15 mL conical tube. The cells were washed 3 times with cold 1X PBS. In each washing step, the cells were spun down at 1,000 rpm for 3 mins. Then cell clusters were dissociated and counted using a Neubauer chamber. A pellet corresponding to 5 x 10^6 cells were transferred to a 1.5 mL Eppendorf tube, spin down at 2,000 g for 10 mins and stored at -80 ^{o}C immediately.

Isolation and purification of RNA

Total RNA was isolated and purified using Qiagen's miRNesy mini kit (Cat. 217004) according to manufacturer's instructions. The yield of RNA extraction and its purity were determined by a Thermo Scientific Nanodrop 2000 spectrophotometer (Waltham, MA). The average absorbance ratio at 260/280 nm for all samples were 2.08 ± 0.03. As seen in **figure 8**, the RNA integrity was further assessed using a Bioanalyzer 2100 with RNA 6000 Pico chips

resulting in RIN scores > 9 (Agilent Technologies). Total RNA (5µg) was aliquoted for immediate digestion and the remaining sample was stored at -80 °C.

Figure 8. A representative electrophoretogram of LNZ-308 obtained on Agilent Bioanalyzer 2100 RNA 6000 Pico Chip (RIN = 9.2).

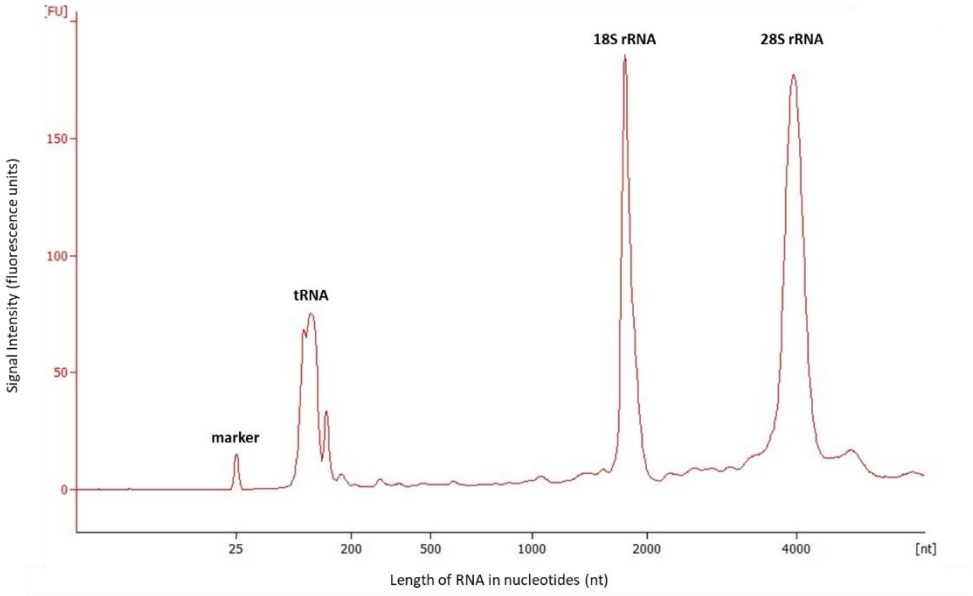

Enzymatic digestion of total RNA to monomeric nucleosides

Each RNA sample (5µg) was digested into monoribonucleosides in a 25 µL enzymatic reaction following a previously published report[198]. In brief, the reaction mixture contained: 0.1 unit of phosphodiesterase I (US Biological, #P4072), 1.0 unit of alkaline phosphatase from E. coli (Sigma-Aldrich, P5931), 10 units of Benzonase (Sigma-Aldrich, E8263), 50 mM of Tris-HCl (pH 8.0), 1 mM of $MgCl_2$ and 0.1 mg/mL of BSA (Sigma-Aldrich, St Louis, MO). The reaction was incubated at 37 °C for 3 hrs. The enzymes were then removed by filtration in a pre-rinsed spin filter (Omega Nanosep 3K MWCO, Pall Corporation, Port Washington, NY) at 14,000 g and 4°C for 30 mins. The digested RNA sample was diluted to 50 ng/µL in Optima grade water containing 0.096 ng/µL leucine enkephalin as an internal standard. A heavy labeled adenosine $^{13}C_{10}$,$^{15}N_5$ internal standard was tested but signal fluctuations due to trap capacity was identified. Bioanalyzer results validated digestion efficacy.

Sample Stability

To address the possibility of variation due to chemical stability total RNA from the GBM model LNZ-308 was isolated, aliquoted, and stored at -80°C. Each LC-MS/MS analysis as detailed above occurred monthly for three consecutive months. A freshly acquired cellular sample was used as the control. The signal for each detectable modified ribonucleoside was constant over time (**Figure 9**). In comparison to the results obtained from the fresh sample, the average percentage difference in signal intensities for all detectable modified ribonucleosides over three months was ~4%. Overall, from the viewpoint of chemical stability, these results show that the GBM epitranscriptome is sufficiently stable and supports its use in these studies.

Figure 9. Extracted ion chromatograms of GBM epitranscriptome (LNZ-308). The RNA sample was extracted from a GBM cell culture, digested and aliquoted. The epitranscriptomic analysis was repeated periodically over three consecutive months. Each peak corresponds to one of the modified ribonucleosides detected in the selected GBM epitranscriptome.

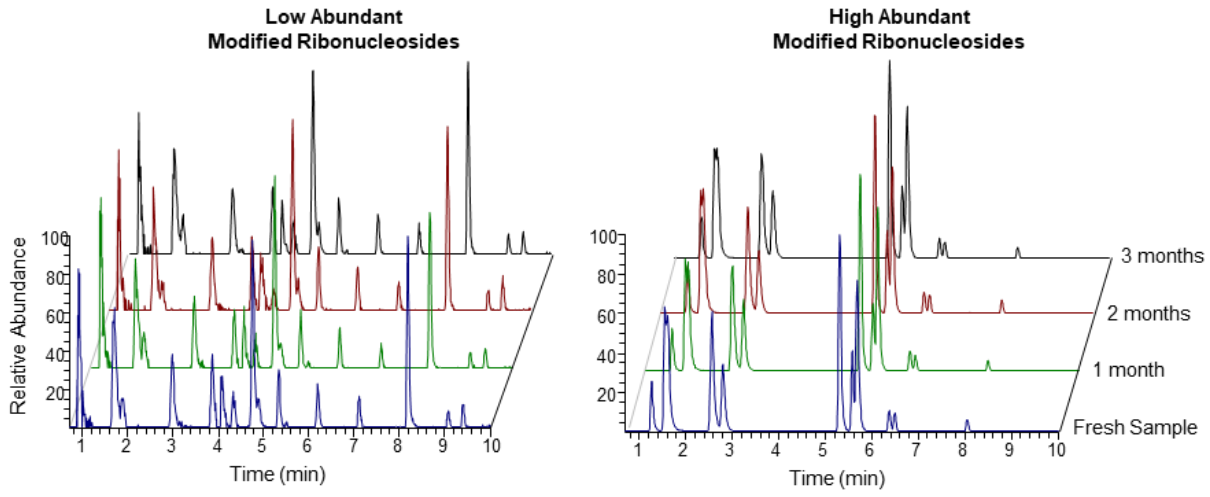

UPLC-PDA-MS/MS analysis of nucleosides

Chromatographic separation of ribonucleoside standards or digested RNA samples was performed on an Acquity ultra-performance liquid chromatography (UPLC) system (Waters Corporation, Milford, MA) with a binary pump and an autosampler maintained at 4 °C. A Water's Acquity UPLC HSS T3 column (2.1 x 50 mm, 1.8 µm particle size) and a HSS T3

VanGuard pre-column (2.1mm x 5 mm, 1.8 µm particle size) with an Acquity inline filter kit held at 30 °C were used. After injecting 10 µL of sample onto the column, the elution was carried out with a two-solvent system prepared with Optima grade solvents. Mobile Phase A consisted of H_2O with 0.01 % formic acid and Mobile Phase B consisted of 50 % CH_3CN with 0.01 % formic acid held at flow rate of 0.4 mL/min. The binary elution gradient was carried out as follows: an initial isocratic composition of 100:0 (A:B) from 0.0 – 0.5 min., increasing to 70:30 from 0.5 – 9.0 min. at a curve of 7, linearly changing to 50:50 from 9.0 - 10.0 min., followed by another linear increase to 0:100 from 10.0 – 15.0 min., a final isocratic hold at 0:100 from 15.0 – 16.0 min. marks the transition to column wash and re-equilibration at the starting conditions for 8 minutes. An inline Water's Acquity eλ photodiode array (PDA) detector collected spectra across a wavelength range of 190 – 340 nm.

High resolution tandem mass spectrometry (MS/MS) was performed on a Q Exactive Plus mass spectrometer (Thermo Fisher Scientific, Waltham, MA) in the positive mode with a heated electrospray ionization source (HESI) with heater temperature at 425 °C, capillary temperature 275 °C, and spray voltage at 3.5 kV. Sheath and auxiliary gas flow were set at the arbitrary values of 50 and 13, respectively. Mass spectra were collected using two scan events. The first scan was a full scan between 100 – 700 m/z at a resolution of 70,000. The second scan employed an inclusion list of the calculated m/z of all known RNA modifications as reported in the Modomics database with a 1.0 m/z isolation window[77]. A two-step higher-energy collisional dissociation (HCD) fragmentation of the top 5 most abundant precursors was employed at normalized collision energies (NCE) of 20 and 110 at 17,500 resolution. Prior to each experiment, mass calibration was performed using a canonical ribonucleoside standard mixture (3.25 µM) with an error of <1 ppm and retention time accuracy ± 0.1 min.

Each RNA sample was analyzed in triplicate and blanks were used between repeated measurements. If multiple RNA samples were analyzed in the same experiment, the order of the repeated measurements was randomized.

Validation of LC-MS/MS Methodology

To demonstrate the reliability of our LC-MS/MS method with complex sample sets, intra-lab method validation of repeatability and trueness were carried out by following the United States Food and Drug Administration (USFDA) standards for bioanalytical methods. Repeatability expresses the closeness of results in a single run or injection and is defined in terms of percent relative standard deviation (RSD). In terms of LC-MS/MS precision the expected RSD for each measurement should be less than 15% deviation from the mean of the integrated peak area, except for the lower limit of quantitation which should be less than 20% deviation from the mean. Intermediate precision, also known as intra-lab reproducibility, is a measure of precision obtained over three different, non-sequential runs. The intermediate precision is calculated by pooled RSD which is a weighted root mean square average of RSDs, where the numbers of degrees of freedom of the individual RSDs serve as weights. According to the International Vocabulary of Metrology, trueness is defined as the closeness of agreement between the average of an infinite number or replicate measured quantity values and a reference quantity value. As a determination of trueness, we compared the linearity and selectivity of 8 calibration curves with the 2X dilution curves of a GBM cell model LNZ-308 for the same RNS.

As to the first question of can we quantify? Eight calibration curves made up of the analytical standards of four canonical RNS (adenosine, cytidine, guanosine, and uridine) and 4 additional modified RNS (m5C, m2,2G, m5Um, and mcm5s2U) were measured and repeated in triplicate. The limit of detection (LOD) for the representing ribonucleosides was in the fg/µL concentration range, the limit of quantitation (LOQ) was in the fg/µL to pg/µL range for all calibrants with coefficients of determination (r^2) values ≥ 0.9997 (**Table 1**). Intermediate Precision, or our intra-lab reproducibility, was measured for the same 8 RNS in concentrations inside the working range between standards and dilutions over 3 non-concurrent days with

RSDs that range from 0.4 to 5.5 % (**Table 2**). Due to the low abundance of m5Um and mcm5s2U in LNZ308 the points used were limited, but within the linear dynamic range.

Table 2. Regression parameters for selected ribonucleoside standards.

Abbreviation	Calibration equation	LOD (fg/µL)	LLOQ (pg/µL)	Linear Range (pg/µL)	R^2	RT (±0.1min)	$[M+H]^+$
A	y = 5E+08x + 5E+06	< 95.4	12.2	156 -12.2	0.9997	4.6	268.1040
C	y = 3E+08x - 71426	95.4	0.763	391-0.763	0.9997	0.9	244.0929
G	y = 2E+08x + 1E+06	95.4	6.10	156 - 6.10	0.9998	4.1	284.0992
U	y = 5E+07x + 17396	191	1.56	391 - 1.56	0.9999	2.1	245.0774
m5C	y = 5E+08x + 22788	< 95.4	0.191	97.7 - 0.191	0.9999	1.7	258.1087
m2,2G	y = 5E+08x - 57620	< 95.4	0.191	97.7 - 0.191	0.9998	6.5	312.1308
m5Um	y = 2E+08x - 18540	< 95.4	0.191	48.8 - 0.191	1.0000	6.2	273.1084
mcm5s2U	y = 2E+08x - 21970	191	0.382	48.8 - 0.382	1.0000	7.1	333.0757

Table 1. Intermediate precision determined by pooled RSD over 3 non-recurrent days

2X Dilution	A	C	G	U	m5C	m2,2G	m5Um	mcm5s2U
256	1.5%	2.0%	3.3%	0.6%	2.6%	0.8%		
128	0.4%	0.7%	2.5%	4.6%	2.1%	1.9%		
64	1.7%	2.1%	2.7%	2.7%	2.4%	2.5%		
32	3.0%	1.8%	1.9%	2.5%	2.1%	0.6%		
16	2.8%	2.8%	1.4%	1.5%	2.2%	0.7%	1.5%	
8	1.0%	5.5%	2.3%	0.8%	2.0%	0.6%	1.2%	3.0%
4	1.9%	3.1%	1.2%	0.7%	1.5%	1.7%	1.1%	1.2%
2	3.1%	6.0%	2.1%	3.0%	0.5%	2.3%	0.8%	1.3%

The next question addressed was can we quantify selectively? Selectivity is defined by IUPAC as the extent to which other substances interfere the determination of a substance according to a given procedure. Matrix effects are a type of bias that arises in a complex mixture that may suppress or enhance analyte ionization by co-eluting compounds. Linearity is the linear relationship between concentration and analyte signal of the standards and analyte concentrations of samples in matrix conditions. To test for selectivity, we explored the signal response of the same eight calibrants listed above against their corresponding signal response in the LNZ-308 dilution curves ran on different days (**Figure 10**). The black squares represent the standard curves while the blue circles represent the LNZ-308 dilutions. All coefficients of determination (r^2) values are > 0.9994. The X axis is the reciprocal dilution factor while the y axis is the relative intensity where both axes have been log10 scaled to show linearity.

Figure 10. Evaluation of trueness by comparison of standard curves and sample dilution curves for linearity and selectivity. Curves were acquired on nonconsecutive days with r^2 values > 0.9994. The y axis is reported in Log10 scaling and x axis is the reciprocal of the 2X dilution factor. Black squares represent the standard curves while blue circles represent LNZ-308 dilution curves.

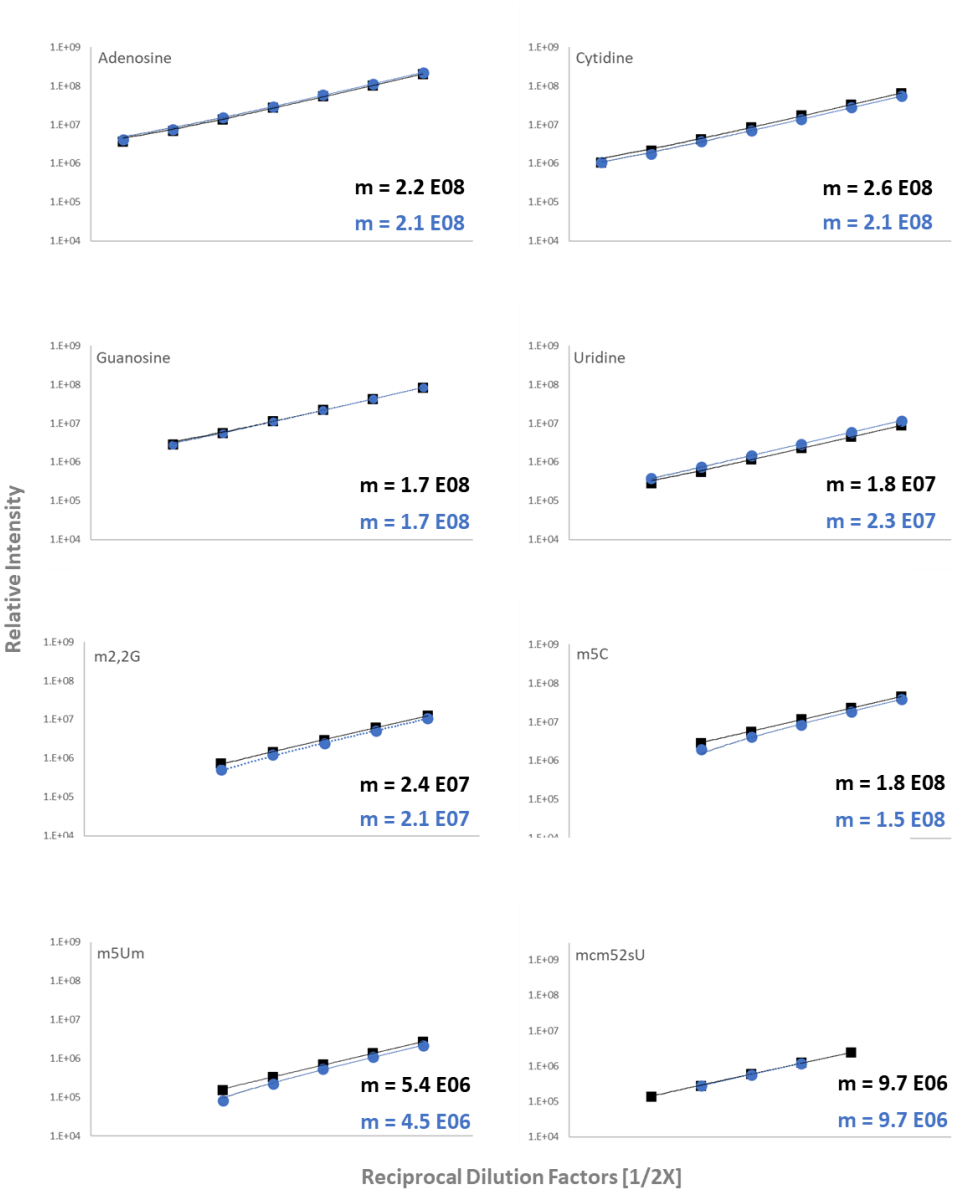

CHAPTER III: THE GLOBAL EPITRANSCRIPTOMIC PROFILE OF GBM

Introduction

Technological advancements in characterizing and quantifying the epitranscriptome via NGS and LC-MS/MS approaches have broadly expanded the biological relevance of RNA modifications and their associated RMPs on health and disease. However, most studies are narrowly focused on the seven RNA modifications identified in mRNA using NGS techniques. It is well known that the more heavily modified noncoding RNAs can also induce regulatory control mechanisms suggesting the importance of the entire epitranscriptome on phenotypic expression[199]. To highlight this further, new reports have confirmed epitranscriptomic crosstalk for the first time [134,135]. The monitoring of RNA modifications in all classes of RNA as well as specific transcripts will be invaluable for elucidating the role of the epitranscriptome in phenotypic modulation. To date, there are minimal characterization or comparative studies for all RNA modifications in a specific biological system. Basanta-Sanchez et al. analyzed the epitranscriptome of human pluripotent stem cells undergoing differentiation[200]. In 2016 the Fabris lab identified a modulated epitranscriptome expression profile of *S. cerevisiae* as a stress response when grown under hyper-osmotic and heat shock conditions[201]. Yoluç and coworkers report these profile changes are linked to pre-existing tRNAs. They also state that RNA transcription and especially activity rates of RMPs were the cause with no change little change to 18S and 25S rRNA[202]. In collaboration with Prof. David Mills at the University of California Davis, we showed a global epitranscriptomic downregulation in the gut microbe *Lactobacillus agilis* as part of cellular response to the adaption of a new food source, namely the prebiotic inulin[203]. The collaborative work of Peter Dedon has focused on RNA modifications in malaria and tuberculosis exposing tRNA codon biased translation during stress response[204–206]. However, there are no reports to date regarding a phenotypic specific global epitranscriptome in cancer or GBM specifically although multiple individual modifications have been identified.

Analysis of the Global Epitranscriptomic Profile in GBM Cells

By using the LC-MS/MS method described in the last chapter, the epitranscriptome of immortalized GBM cell lines LNZ-308 and U87 were profiled and found 32 different RNA modifications were detected (**Table 3**). Previously described UPLC high resolution MS/MS parameters were employed. Biological and technical replicates were used to account for variation and precision (n=3, RSD 0.1 – 7.7%). All 32 modified RNS were identified through accurate mass analysis (0.3 – 1.5 ppm), precise retention time (RT ± 0.1 min), two-step HCD MS^2 fragmentation, and *in silico* fragmentation with Mass Frontier Spectral Interpretation Software (Thermo Fisher Scientific, Waltham, MA, USA) (**Figure 11 and Table 3**). Spectral databases were also used as secondary confirmation when standards were not available including: MassBank of North America, mzCloud, Human Metabolome Database, and Metlin.

Figure 11. A representative comparison of an acquired MS2 spectra with predicted in silico fragmentation. A) Two step HCD MS^2 spectra of m6A from GBM model LNZ-308 generated on a Thermo Q Exactive Plus orbitrap MS. B) In silico MS^2 fragmentation prediction of m6A.

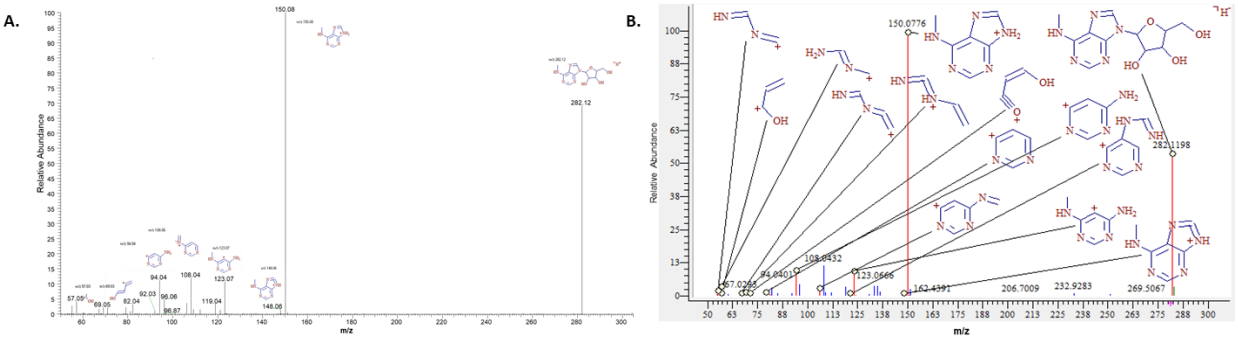

Table 3. Repeatable RNA modifications identified in GBM models LNZ-308 and U87

RNS	RT (± 0.1 min)	Formula	m/z	Accuracy (ppm)	Precision (% RSD)	Fragment Ions
Y	1.0	$C_9H_{12}O_6N_2$	245.0771	1.050	0.6	209.0557,179.0451,155.0452
D	0.9	$C_9H_{14}O_6N_2$	247.0928	1.527	5.7	115.0506,97.0289
m1acp3Y	1.9	$C_{14}O_8N_3H_{21}$	360.1403	0.330	6.0	360.1405,324.1192,294.1081,270.1086,223.0715, 228.4908
m3C	1.3	$C_{10}O_5N_3H_{15}$	258.1086	0.747	2.7	126.0664,109.0401,95.0246,82.0294,56.9657
m1A	1.6	$C_{11}O_4N_5H_{15}$	282.1199	0.778	0.5	282.1197,150.0775,133.0510,109.0513
m5C	1.7	$C_{10}O_5N_3H_{15}$	258.1087	1.096	0.2	126.0661,109.0398,83.0609,56.0503
acp3U	1.7	$C_{13}O_8N_3H_{19}$	346.1248	1.008	0.2	346.1246,214.0823,197.0561,168.0768,96.0085,56.0504
ncm5U	1.9	$C_{11}O7N_3H_{15}$	302.0988	1.42	6.5	170.0565
m7G	2.7	$C_{11}O_5N_5H_{17}$	298.1149	0.956	3.3	298.1147,166.0724,149.0458,124.0508,69.0455
Cm	2.9	$C_{10}O_5N_3H_{15}$	258.1087	0.980	0.4	112.0509,95.0245,69.0455
m1Y	3.1	$C_{10}O_6N_2H_{14}$	259.0927	1.07	0.8	169.0608,179.0452,227.0650,209.0551
I	3.9	$C_{10}O_5N_4H_{12}$	269.0883	0.758	3.9	137.0459,119.0355,110.0353,56.9656
m5U	4.1	$C_{10}O_6N_2H_{14}$	259.0927	0.723	2.5	127.0504,110.0241,84.9603,56.9656
Um	4.8	$C_{10}O_6N_2H_{14}$	259.0928	1.341	0.1	113.0349,147.0652,96.0085,70.0295
m3U	4.9	$C_{10}O_6N_2H_{14}$	259.0928	1.148	0.8	127.0504,96.0085,84.9604,56.9656
m1G	5.4	$C_6H_8ON_5$*	166.0724	0.563	3.2	166.0724
Gm	5.4	$C_5H_6ON_5$*	152.0568	0.55	1.3	152.0568
m1I	5.4	$C_{11}O_5N_4H_{14}$	283.1039	0.791	0.4	151.0616,110.0352,82.0406,56.9656
mcm5U	5.6	$C_{12}O_8N_2H_{16}$	317.0984	1.102	7.0	185.0561
m2G	5.6	$C_{11}O_5N_5H_{15}$	298.1148	0.788	0.9	298.1144,166.0725,149.0458,135.0302(loss of CH5N),128.0456,110.0353
ac4c	5.7	$C_{11}O_6N_3H_{15}$	286.1035	0.588	0.8	154.0612,112.0509,95.0246,69.0455
Am	5.7	$C_{11}O_4N_5H_{15}$	282.1199	0.814	1.0	282.1198,136.0619,119.0356,92.0250,67.0299
m2,2,7G	5.8	$C_{13}O_5N_5H_{21}$	326.1462	0.935	0.5	194.1038,167.0565,124.0508
m5Um	6.2	$C_{11}O_6N_2H_{16}$	273.1083	0.649	1.2	127.0504,110.0242
m6A	6.4	$C_{11}O_4N_5H_{15}$	282.1199	0.991	0.7	282.1198,150.0775,123.0668,133.0508,108.0435,94.0406
m2,2G	6.5	$C_{12}O_5N_5H_{17}$	312.1304	0.560	2.4	312.1299,180.0880
mcm5s2U	7.1	$C_{12}O_7N_2H_{16}S$	333.0754	0.877	1.9	201.0329,169.0067,141.0116
m6Am	7.4	$C_{12}O_4N_5H_{17}$	296.1356	0.842	0.2	296.1356,150.0775,108.0434,94.040
m6,6A	8.1	$C_{12}O_4N_5H_{17}$	296.1356	0.91	0.1	296.1354,164.0932,120.0433 (loss of C2H6N)
t6A	8.2	$C_{15}O_8N_6H_{20}$	413.1421	1.239	0.2	281.0994,162.0410,136.0618,119.0355
m6t6A	9.0	$C_{16}O_8N_6H_{22}$	427.1578	1.456	1.0	295.1149,150.0776,123.0669,108.0435
ms2t6A	9.4	$C_{16}O_8N_6H_{22}S$	459.1298	1.353	2.1	327.0869,208.0288,134.0463
i6A	10.7	$C_{15}O_4N_5H_{21}$	336.1668	0.623	7.7	336.1667,204.1245,136.0618,148.0618

Validation of global epitranscriptomic profile of GBM sensitive to chemotherapeutics

Following the standard of care treatment, GBM will reoccur and develop resistance to treatment. Intratumoral heterogeneity is a main determinant of treatment failure and recurrence due to the divergent cells within a tumor that express variant phenotypic states, including GSCs. GSCs are considered the source of tumor initiation and recurrence since GSCs maintain neural stem-like properties such as self-renewal and differentiation. Unfortunately, histological and genetic dissimilarities have been noted in multiple model cell lines[207]. Preclinical cell lines that

maintain these same traits are essential for understanding GBM biology and effective treatment strategies to overcome the inevitable resistance to current treatments[208–210]. It can be difficult to attain low passage, serum-free, patient derived stem-like cell lines that cover all three GBM subtypes. We are fortunate to have access to them through our collaboration with Prof. Bakhos Tannous.

Once a repeatable profile was identified in immortalized GBM cell lines, patient derived primary cells sensitive to TMZ (MGG6, GBM8, and PN157) were used to further confirm the list of RNA modifications detected in the GBM epitranscriptome. Healthy controls consisted of pooled total RNA from 5 human donors with no history of cancer (BioChain, Eureka, CA, USA), neural stem cells and fibroblast cells were again provided by Dr. Bakhos Tannous. Unsupervised analysis of the global epitranscriptomic datasets was performed using the multivariate statistical approach, principal component analysis (PCA) generated by MetaboAnalyst, a web-based metabolomic data analysis platform[211]. PCA is used to explain variance in data sets containing many variables without consideration to classifications. These uncorrelated variables, or principal components, are ordered into a series of decreasing variance reducing data dimensions and capturing visual patterns within the data. The PCA scores plot shows the relationship between samples, whereas the loadings plot shows the weighting of the individual variable to a particular principal component. The MS epitranscriptomic data evidenced a correlation of the GBM samples within a 95% confidence interval. The samples deemed as healthy controls were spatially separated correlating within a separate 95% confidence interval (**Figure 12A**). Another unsupervised method, hierarchical clustering analysis (HCA) is a type of agglomerative or “bottom-up” clustering that starts with regarding each element as an individual cluster that successively merges each cluster until they all belong to one cluster. Two parameters considered with HCA are similarity or correlation measurements along with clustering algorithms which are then represented by a dendrogram. The samples defined as healthy controls and GBM clustered individually. The healthy controls

further grouped with the neural stem cells and fibroblasts being more similar than the RNA from the 5-person donor pool. Within the GBM grouping, the immortalized lines grouped separately from the patient derived primary cell lines and further the GBM8 and PN157 were more similar than MGG6 (**Figure 12B**). Overall, a phenotypically repeatable set of RNA modifications were detected with subtle differences in abundance highlighting the need for more accurate quantitative methodologies. This is especially important considering small changes in RNA modifications can be biologically relevant.

Figure 12. Unsupervised statistical analysis of GBM epitranscriptome. A) PCA scores plotting of GBM and HC samples generated using MetaboAnalyst. The 95% confidence intervals are indicated by elliptical shading. B) HCA clustering with similarity measurements by Pearson's correlation and clustering algorithm using Ward's linkage generated by MetaboAnalyst.

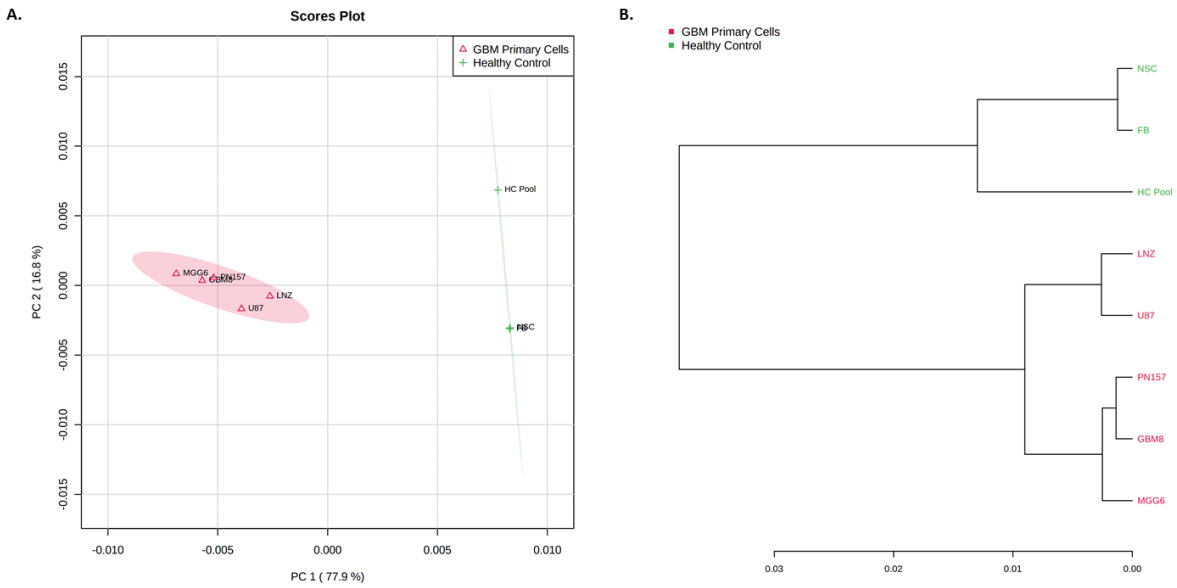

CHAPTER IV: STANDARD-FREE QUANTITATIVE EPITRANSCRIPTOMIC PROFILING OF RNA MODIFICATIONS

Introduction

The role of RNA modifications in human disease is gaining rapid interest since epitranscriptome not only alters RNA structures and functions, but also interacts with other cellular molecules[212–214]. Despite >150 RNA modifications[77], most studies focus on only one specific RNA modification while the transcriptomes are decorated with many others, which may individually or combinatorically affect RNA-dependent cellular activities[83,215,216]. The lack of comprehensive epitranscriptomic studies is partly due to the analytical challenges in profiling the full spectrum of RNA modifications in a given epitranscriptome[200,217,218].

Mass spectrometry (MS) is the most accurate technique for characterizing RNA modifications[167]. However, to achieve absolute quantification of each modified ribonucleoside, multiple standards are required, some of which are not commercially available. To achieve relative quantification of RNA modifications, two different methods are commonly used. In the first method (M-1), the signal of a specific modified ribonucleoside is normalized to its corresponding canonical ribonucleoside (CR). In the second method (M-2), the modified ribonucleoside signal is normalized to the sum of all four CR detected in the same sample[12–14]. The use of endogenous CR to normalize the epitranscriptomic data is logical when a high percentage (~90%) of the transcriptome are unmodified and remain constant. For MS measurements, the ionization efficiency (IE) of compounds with different molecular structures are not expected to be equal, and result in different signal intensities. Therefore, with the diverse chemical structures involved in RNA modifications, the normalized signals with both M-1 and M-2 methods are potentially biased. For comparative analysis (e.g. diseased vs healthy), the error in the normalized signals resulting from differences in IE can become even worse unless a suitable control sample with matching percent composition of CR is used. The percent

composition of CR in each sample of interest can be unique representing a challenge with the current normalization methods (**Figure 13**).

Figure 13. Variations of percent composition of canonical ribonucleosides found in 5 GBM cell lines and healthy control. Results were determined by corresponding standard curves.

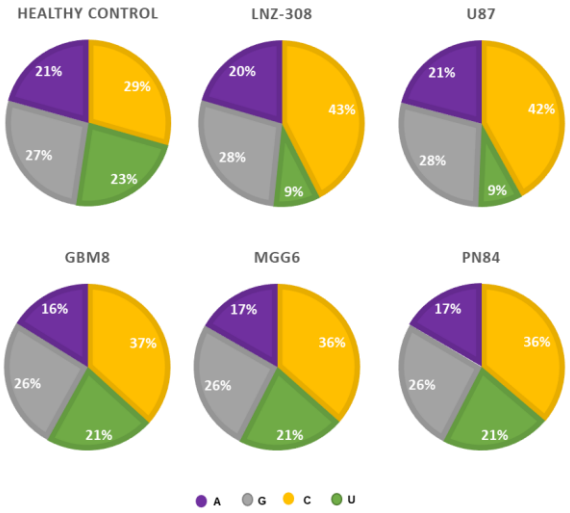

The effects of divergent ionization efficiencies on reported normalization methods

To determine the effects of IE and the percent composition of CR on the current methods, three different standard mixtures were prepared, as detailed in **Figure 14**, where in each sample, the amount of two selected RNA modifications (Am and Y) was equal. We then applied the current methods to normalize the signal of each selected modification. When M-1

Figure 14. The percent distribution of selected ribonucleoside standards in three different mixtures. A = adenosine, U = uridine, G = guanosine, C = cytidine, Am = 2'-O-methyladensoine, Y = pseudouridine. The amount of Am = Y in all mixtures.

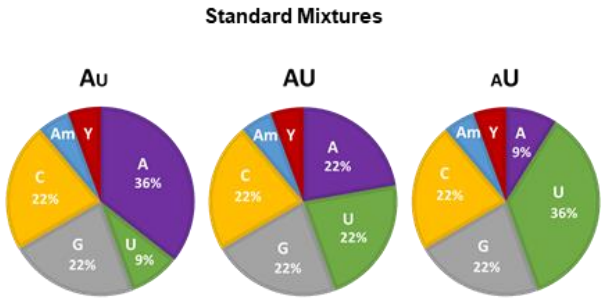

was applied, Y was shown to be more abundant than Am in two different mixtures (Au and AU) while the third mixture (AU) showed the opposite effect (**Figure 15**). On the other hand, M-2 resulted in Y being much lower than Am in all mixtures. To simulate the possible changes in the percent composition of CR, the corresponding CR of Am and Y, namely adenosine and uridine, were varied while the total mass in each standard mixture was kept constant. Both M-1 and M-2 methods failed to report the equal amount of Am and Y (**Figure 15**). This error in the normalized value would affect studies focusing on either a single or complete profile of RNA modifications in each epitranscriptome.

Figure 15. Results obtained from using either M-1 or M-2 method to normalize the MS signals of Am and Y in the three standard mixtures. Data presented as mean ± SD (n = 3); *p < 0.05; **p < 0.01; ***p < 0.001, two-tailed student's t-test.

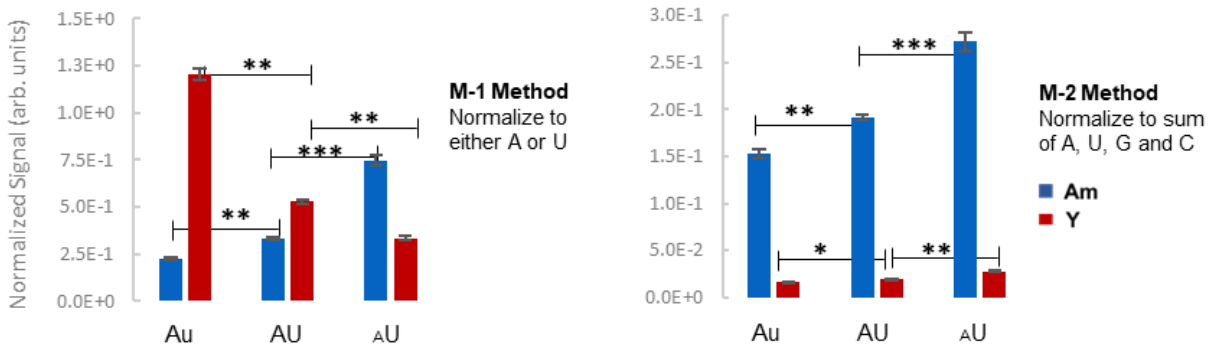

Negating the effect of ionization efficiencies in epitranscriptomic quantitation

To overcome the inaccuracies associated with current methods, we developed a standard-free quantitative epitranscriptomic profiling method, named Squared EP (SqEP). Based on the principle of electrospray ionization MS (ESI-MS)[219], the sensitivity of measuring different chemical compounds is proportional to their IE, which in turn correlates with the slope of their corresponding standard curves. The higher the IE, the steeper the slope, and vice versa. In the SqEP method, an adjustment factor is calculated for each ribonucleoside in relation to the most ionizable CR

Figure 16. Schematic diagram summarizing the principle of the SqEP method. In the first step adjustment ratios for all ribonucleosides are defined. In step 2, the MS signal is adjusted by multiplying the signal with an adjustment factor. The final SqEP value is further adjusted by the sum of the 4 adjusted canonicals.

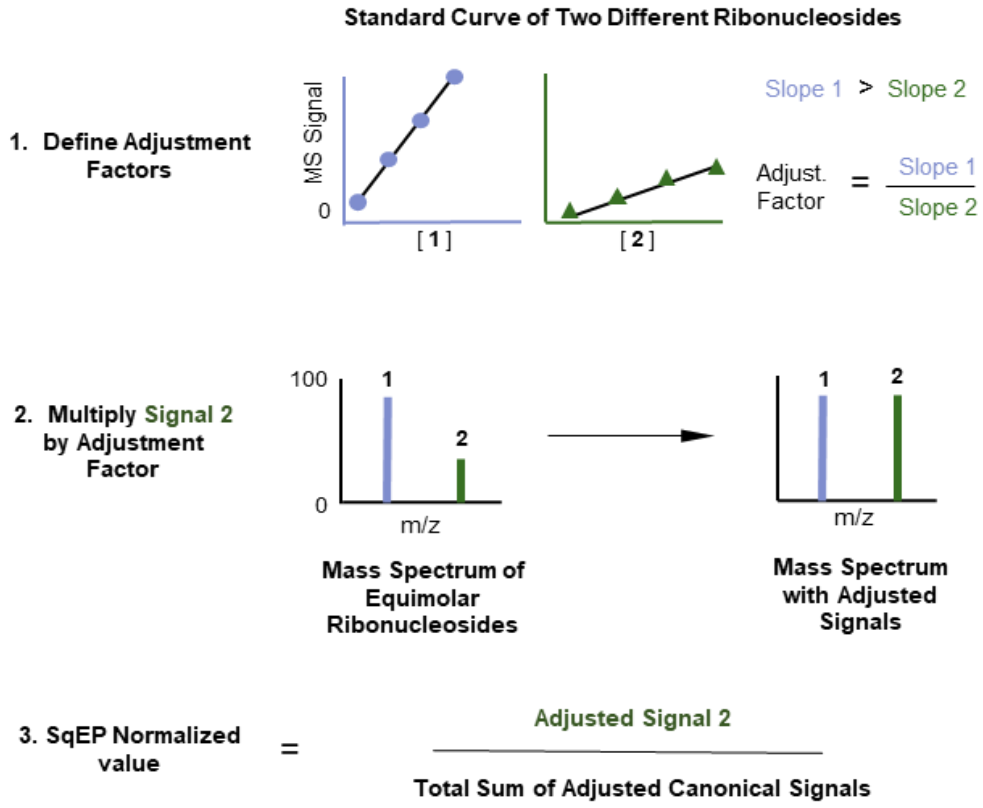

with the aim of counterbalancing the differences in IE between different ribonucleosides (**Figure 16**). Specifically, the adjustment factor of each ribonucleoside is calculated by dividing the slope of adenosine standard curve with the slope of each ribonucleoside (**Table 4**). When using the SqEP method, the raw MS signal of each ribonucleoside is first adjusted by multiplying it with the corresponding adjustment factor. To confirm that the differences in IE are canceled out, we plotted the adjusted signals in each calibration experiment and showed that the curve for all ribonucleosides overlaps with an identical slope (**Figure 17**). To account for systematic bias introduced during sample preparation and data acquisition, a subsequent normalization step is applied in SqEP, where the adjusted signal of each ribonucleoside is normalized to the sum of adjusted signals of all four CR (**Figure 16**). Using the SqEP method to re-analyze the raw MS

Figure 17. Overlay of adjusted standard curves. The MS signal of each standard was adjusted by multiplying it with the corresponding adjustment ratio (Table 4). The adjusted standard curves have an identical slope.

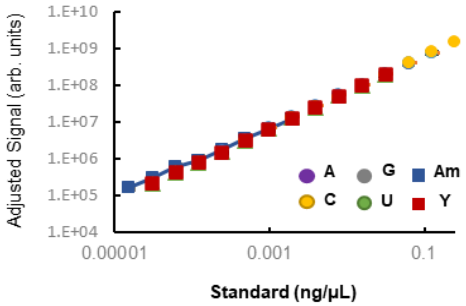

signals obtained from the three standard mixtures in **Figure 14**, we showed that all normalized signals of Am and Y complied with their actual concentrations, irrespective of differences in the concentration of corresponding CR (**Figure 18**). Overall, despite the differences in IE, our SqEP method can be used to determine whether specific RNA modifications are up- or down-regulated among different samples without the need to identify a suitable control with matching percent composition of CR. In addition, our method can be used to rank the abundance of all detectable RNA modifications in a given sample, which is important when studying possible relationships between different RNA modifications.

Table 4. Summary of the results from performing the calibration with the selected ribonucleoside (RNS) standards in Figure 14

RNS	Equation of Linear Regression	R^2	LOQ* (nM)	Linear Range (nM)	Adj. Factors
C	y= 106130711.41x - 142726.21	0.9997	1.53	1.53 - 3125	1.00
A	y= 192158023.08x + 4080617.89	0.9994	3.05	3.05 - 3125	7.34
G	y= 83204911.87x + 1327943.24	0.9987	1.53	1.53 - 6250	1.81
U	y= 26163350.70x + 152531.55	0.9995	3.05	3.05 - 6250	2.31
Am	y= 295658058.59x + 4549203.29	0.9995	1.53	1.53 - 3125	0.65
Y	y= 31703987.91x - 965830.75	0.9990	6.10	6.10 - 6230	6.06

*The limit of quantitation (LOQ) was determined to be the lowest concentration with residuals calculated at < 15%.

Figure 18. Results obtained by using SqEP method to normalize the MS signals of Am and Y in the three standard mixtures.

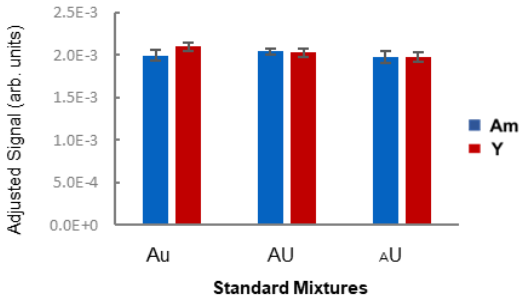

Working around a lack of standards in epitranscriptomic profiling

The main challenge for full epitranscriptomic analysis is the lack of pure standards to construct all standard curves required for calculating the adjustment factor of each detectable RNA modification. To overcome this issue, we explored the possibility of constructing a dilution curve for each detectable RNA modification, from which the slope ratio can be obtained. As a proof of concept, we profiled the epitranscriptome of LNZ-308 glioblastoma (GBM) cell line as a model. Digested ribonucleosides were serially diluted, analyzed by ultra-performance liquid chromatography (UPLC)-MS, and raw MS data were used to generate a dilution curve for each ribonucleoside. By comparing the dilution curve to their corresponding standard curve, we found that both slope values are comparable (**Figure 19a-b**). The criteria for constructing each dilution

Figure 19a-b. Overlay of the standard curve with its corresponding dilution curve. In the latter case, results were obtained from a series of dilutions prepared from a GBM sample (LNZ-308). m = slope of regression analysis

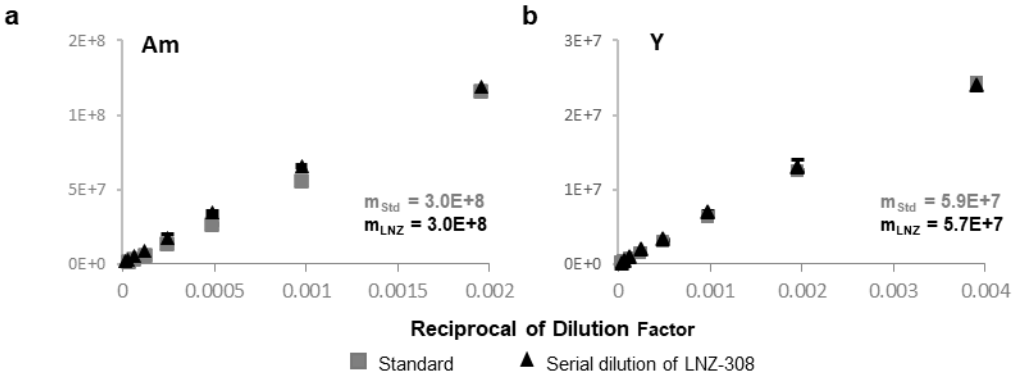

curve is that the corresponding ribonucleoside must be detectable in at least three dilutions of the selected sample. To obtain an accurate slope value, the undiluted concentration of each ribonucleoside must be determined and used in plotting each dilution curve. This was achieved by carrying out post-column UV detection on the UPLC-MS platform. With the measured UV absorbance and the molar absorptivity available in the literature, the undiluted ribonucleoside concentration was calculated. Overall, the results indicate that the dilution curve slope matches with the corresponding slope value obtained using the standard curve with an average difference of only 3.6% (**Table 5**) [9]. For modified ribonucleosides with unknown molar absorptivity, we could experimentally derive their values such that their undiluted concentration could be determined. Among the 31 RNA modifications detected in the selected GBM sample, 22 of them have known molar absorptivity available in the literature, thus no ribonucleoside standard was required to determine their undiluted concentration. Together with three additional

Table 5. Validation of adjustment factors obtained from dilution curves.

RNS*	Slopes		Adjustment Factors		
	Standard Curve †	Dilution Curve Δ	Standard Curve	Dilution Curve	% Difference
C	1.06E+08	1.04E+08	1.80	1.77	2%
m5C	1.67E+08	1.53E+08	1.15	1.21	-5%
m3C	1.96E+08	1.93E+08	0.98	0.96	1%
Cm	1.57E+08	1.56E+08	1.22	1.19	2%
U	2.72E+07	2.56E+07	7.04	7.24	-3%
Y	5.92E+07	5.64E+07	3.23	3.28	-2%
m5Um	3.09E+07	2.94E+07	6.19	6.31	-2%
G	8.86E+07	8.54E+07	2.16	2.17	0%
m2,2G	1.26E+08	1.11E+08	1.52	1.66	-9%
A	1.92E+08	1.85E+08	1.00	1.00	0%
m1I	1.61E+08	1.61E+08	1.19	1.15	4%
m1A	1.99E+08	2.10E+08	0.96	0.88	8%
m6A	2.10E+08	2.21E+08	0.91	0.84	8%
Am	2.95E+08	3.00E+08	0.65	0.62	5%

* A list of 14 ribonucleoside (RNS) standards of RNA modifications that were detected in GBM epitranscriptome.

† Standard curve of each selected RNS was constructed by using the same experimental approach and criteria as in Supplementary Table 1.

Δ Dilution curve was constructed with the data obtained from the serially diluted GBM samples.

molar absorptivities that were experimentally derived, we obtained the adjustment factor for 25 (out of 31) RNA modifications (81%) from the dilution experiment (**Table 6**). Theoretically, if the same UPLC-MS platform and parameter settings are being used, the same set of 25 adjustment factors can be used for future epitranscriptomic profiling without repeating the dilution experiment.

Table 6. Adjustment factors used in the SqEP method to adjust 25 ribonucleoside signals detected in GBM samples.

RNS	Adjustment Factor*
m5C	**1.21**
m3C	**0.96**
Cm	**1.19**
Y	**6.06**
m1Y	2.62
Um	7.30
m3U	11.41
m5U	**5.04**
m5Um	6.31
mcm5s2U	2.77
m7G	1.20
Gm	2.66
m1G	3.87
m2G	4.53
m2,2G	**1.66**
m2,2,7G	0.41
I	1.22
m1I	**1.15**
m1A	**0.88**
m6A	**0.84**
m6,6A	0.63
Am	**0.65**
t6A	3.88
m6t6A	10.87
ms2t6A	7.23

* Bold = adjustment factors confirmed by using the corresponding standard curves.

The application of SqEP quantitation to GBM models

Finally, we applied the developed SqEP method for epitranscriptome-wide profiling of GBM cells and compared it to currently used methods (M-1 and M-2). We focused on 14 different RNA modifications to which standards are available. Absolute quantification in 2 different GBM cell lines (LNZ-308 and U87 cells), 3 patient-derived neurospheres (PN157, MGG6, MGG8) and a healthy control brain sample, showed that SqEP is superior and more accurate than both M-1 and M-2 in determining the level of different RNA modifications (**Figure 20 and Table 7**). When the complete profile of GBM epitranscriptome (i.e. identity of all detectable RNA modifications and their abundance) is compared with the profile of healthy human brain tissue, a number of RNA modifications were identified to be upregulated in GBM. Both M-1 and M-2 identified different sets of upregulated RNA modifications compared to the SqEP method (**Figure 21a**). Importantly, upregulation of m5C was only identified by the SqEP method, which was also validated using m5C standard curve. According to The Cancer Genome Atlas (TCGA)[220, 17], GBM patients with higher expression of the writer gene for m5C modification had a lower survival rate (**Figure 21b**), supporting the previously reported

Figure 20. Relative abundance of four different RNA modifications in 2 different GBM cells (LNZ-308 and U87) and healthy control brain tissue using M-1, M-2 or the developed SqEP method, in comparison to the corresponding standard curves in absolute quantitation (AQ). m5C = 5-methylcytidine. m2,2G = 2,2-dimethylguanosine.

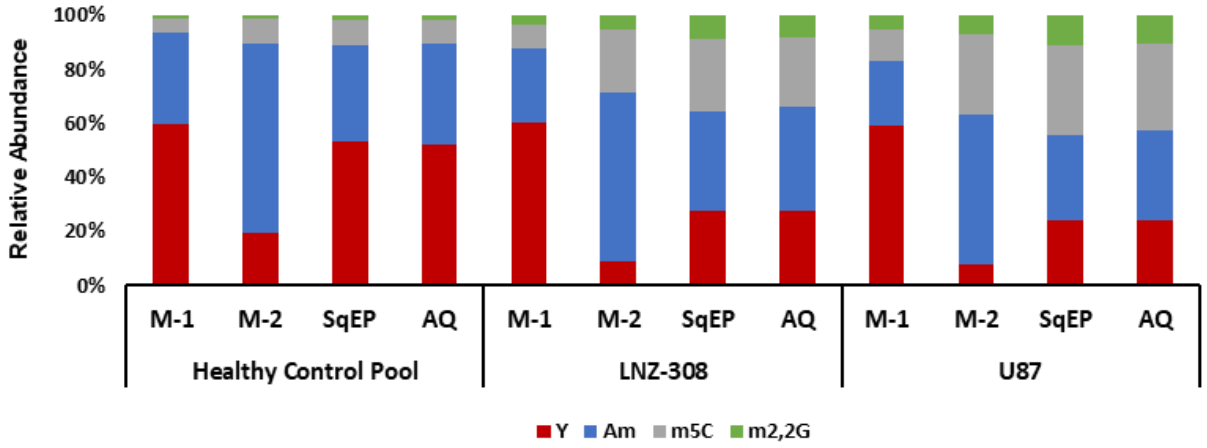

Table 7. Accuracy of using the SqEP method to determine the level of 14 different ribonucleosides (RNS) in the healthy control pool and 5 different GBM cell lines. In each case, the MS signal was normalized to the sum of four canonical ribonucleoside signals is shown.

RNS	Healthy Control Pool			LNZ-308		
	AQ	SqEP	% Diff	AQ	SqEP	% Diff
C	2.94E+03 ± 8.72	2.89E+03 ± 8.08	-1.9%	4.19E+03 ± 65.1	4.13E+03 ± 65.7	-1.3%
U	2.18E+03 ± 50.5	2.24E+03 ± 51.2	2.6%	8.58E+02 ± 1.83	8.85E+02 ± 1.99	3.2%
G	2.69E+03 ± 3.60	2.70E+03 ± 3.15	0.0%	2.83E+03 ± 28.9	2.85E+03 ± 30.1	0.6%
A	2.11E+03 ± 26.9	2.11E+03 ± 26.3	-0.1%	2.03E+03 ± 2.89	2.04E+03 ± 2.16	0.5%
Y	1.34E+02 ± 0.98	1.36E+02 ± 1.02	1.0%	4.00E+01 ± 1.12	4.03E+01 ± 1.13	0.7%
m3C	5.78E+00 ± 0.03	5.96E+00 ± 0.03	3.1%	9.66E+00 ± 0.08	9.82E+00 ± 0.09	1.7%
m1A	6.32E+01 ± 0.17	5.83E+01 ± 0.17	-7.8%	7.84E+01 ± 1.12	7.27E+01 ± 1.04	-7.3%
m5C	2.20E+01 ± 0.48	2.30E+01 ± 0.50	4.4%	3.59E+01 ± 0.12	3.78E+01 ± 0.10	5.3%
Cm	7.63E+01 ± 0.61	7.55E+01 ± 0.59	-1.1%	4.81E+01 ± 0.27	4.82E+01 ± 0.24	0.2%
m1I	6.22E-01 ± 0.07	5.83E-01 ± 0.07	-6.3%	1.53E+00 ± 0.07	1.48E+00 ± 0.06	-3.1%
Am	9.61E+01 ± 3.22	9.25E+01 ± 3.05	-3.8%	5.43E+01 ± 0.41	5.30E+01 ± 0.42	-2.3%
m5Um	7.85E+00 ± 0.06	8.30E+00 ± 0.06	5.7%	3.74E+00 ± 0.04	3.97E+00 ± 0.04	6.3%
m6A	1.95E+01 ± 0.16	1.77E+01 ± 0.14	-9.0%	7.98E+00 ± 0.06	7.36E+00 ± 0.05	-7.7%
m2,2G	4.39E+00 ± 0.09	4.35E+00 ± 0.09	-0.8%	1.16E+01 ± 0.04	1.18E+01 ± 0.05	1.3%

RNS	U87			PN157		
	AQ	SqEP	% Diff	AQ	SqEP	% Diff
C	4.20E+03 ± 10.2	4.14E+03 ± 10.2	-1.3%	4.06E+03 ± 5.09	4.00E+03 ± 4.91	-1.4%
U	8.70E+02 ± 27.0	8.97E+02 ± 27.8	3.2%	1.19E+03 ± 4.83	1.22E+03 ± 5.11	3.1%
G	2.84E+03 ± 6.37	2.86E+03 ± 6.38	0.6%	2.63E+03 ± 18.9	2.64E+03 ± 18.6	0.5%
A	2.09E+03 ± 25.7	2.10E+03 ± 25.9	0.5%	2.22E+03 ± 25.1	2.23E+03 ± 24.9	0.4%
Y	3.61E+01 ± 0.74	3.63E+01 ± 0.74	0.5%	8.56E+01 ± 0.29	8.66E+01 ± 0.28	1.2%
m3C	1.26E+01 ± 0.56	1.28E+01 ± 0.55	1.2%	1.14E+01 ± 0.30	1.16E+01 ± 0.30	1.6%
m1A	9.86E+01 ± 3.26	9.13E+01 ± 3.01	-7.4%	1.15E+02 ± 1.75	1.07E+02 ± 1.60	-7.5%
m5C	4.79E+01 ± 0.91	5.04E+01 ± 0.96	5.4%	3.71E+01 ± 0.28	3.90E+01 ± 0.29	5.2%
Cm	4.52E+01 ± 1.12	4.54E+01 ± 1.10	0.5%	5.20E+01 ± 0.13	5.22E+01 ± 0.14	0.3%
m1I	1.24E+00 ± 0.02	1.20E+00 ± 0.02	-3.6%	1.77E+00 ± 0.02	1.71E+00 ± 0.02	-3.2%
Am	4.96E+01 ± 0.42	4.86E+01 ± 0.39	-2.0%	6.10E+01 ± 1.13	5.96E+01 ± 1.09	-2.3%
m5Um	4.57E+00 ± 0.03	4.86E+00 ± 0.03	6.3%	5.46E+00 ± 0.06	5.80E+00 ± 0.07	6.2%
m6A	8.17E+00 ± 0.19	7.56E+00 ± 0.17	-7.5%	1.46E+01 ± 0.41	1.32E+01 ± 0.36	-9.2%
m2,2G	1.57E+01 ± 0.58	1.59E+01 ± 0.60	1.5%	1.47E+01 ± 0.20	1.49E+01 ± 0.21	1.2%

RNS	MGG6			MGG8		
	AQ	SqEP	% Diff	AQ	SqEP	% Diff
C	3.97E+03 ± 41.0	3.91E+03 ± 40.8	-1.5%	3.93E+03 ± 24.7	3.88E+03 ± 24.4	-1.4%
U	1.27E+03 ± 7.57	1.31E+03 ± 7.68	3.0%	1.15E+03 ± 16.2	1.18E+03 ± 16.7	3.1%
G	2.63E+03 ± 8.58	2.64E+03 ± 8.38	0.5%	2.84E+03 ± 11.3	2.85E+03 ± 11.9	0.4%
A	2.19E+03 ± 35.7	2.20E+03 ± 35.8	0.3%	2.11E+03 ± 0.83	2.12E+03 ± 0.84	0.4%
Y	8.82E+01 ± 1.31	8.93E+01 ± 1.35	1.3%	8.65E+01 ± 0.71	8.74E+01 ± 0.72	1.0%
m3C	1.73E+01 ± 0.71	1.74E+01 ± 0.71	0.2%	1.38E+01 ± 0.18	1.40E+01 ± 0.18	1.8%
m1A	1.31E+02 ± 1.32	1.21E+02 ± 1.22	-7.7%	1.27E+02 ± 2.93	1.18E+02 ± 2.68	-7.5%
m5C	4.30E+01 ± 0.26	4.52E+01 ± 0.26	5.2%	3.57E+01 ± 0.04	3.75E+01 ± 0.04	5.0%
Cm	5.43E+01 ± 0.00	5.41E+01 ± 0.00	-0.3%	5.00E+01 ± 0.17	5.06E+01 ± 0.17	1.2%
m1I	1.87E+00 ± 0.05	1.82E+00 ± 0.05	-2.8%	1.79E+00 ± 0.05	1.72E+00 ± 0.05	-3.7%
Am	6.30E+01 ± 0.17	6.11E+01 ± 0.17	-2.9%	6.01E+01 ± 0.86	5.92E+01 ± 0.83	-1.6%
m5Um	5.62E+00 ± 0.14	5.97E+00 ± 0.15	6.1%	4.89E+00 ± 0.09	5.19E+00 ± 0.10	6.1%
m6A	1.41E+01 ± 0.09	1.27E+01 ± 0.08	-9.7%	1.42E+01 ± 0.35	1.31E+01 ± 0.31	-8.3%
m2,2G	1.64E+01 ± 0.00	1.67E+01 ± 0.00	1.4%	1.48E+01 ± 0.25	1.50E+01 ± 0.25	1.0%

association of upregulated m5C modification in GBM[215,216]. In contrast to the outcome from using the M-1 or M-2 method, the SqEP method showed the level of 5-methoxycarbonylmethyl-2-thiouridine (mcm5s2U) in GBM samples is to be not significantly higher than the healthy control, which complies with the TCGA data on the expression level of the writer gene for mcm5s2U modification (**Figure 21c and Figure 22**). Overall, by removing the biases in normalization, our SqEP method can achieve higher accuracy of epitranscriptome-wide quantification of multiple RNA modifications without the need of any ribonucleoside standards.

Figure 21. GBM epitranscriptomic aberrations. A) Venn Diagram representing the variations and overlap of upregulated RNA modifications detected among five different GBM cells using M-1, M-2 and SqEP methods (Table 6). RNA modifications abbreviated as detailed in the Modomics database. b) Kaplan-Meier survival curve from TCGA database of GBM patients with low (blue) and high (red) level of gene expression of NSUN5, writer for m5C modification. c) TCGA Kaplan-Meier survival analysis of GBM patients with low (blue) and high (red) level of gene expression of CTU1, writer for mcm5s2U modification.

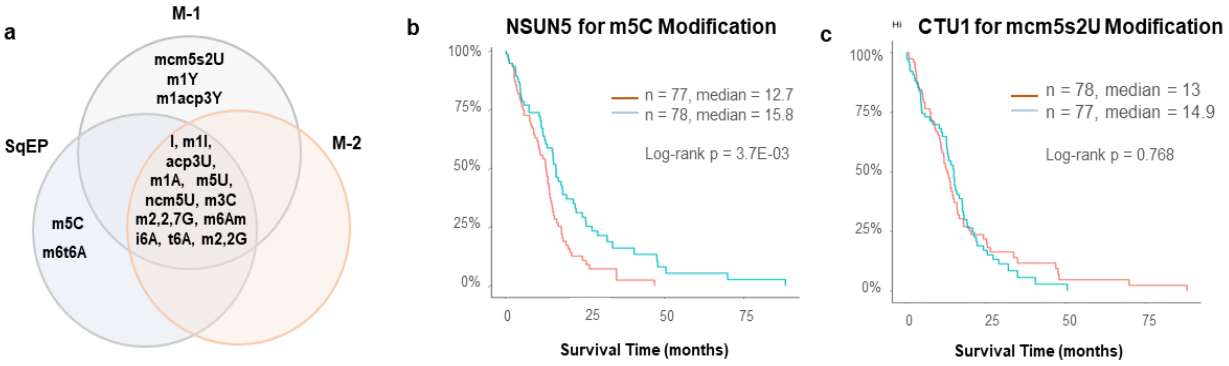

Figure 22. Fold change of mcm5s2U modification between specific GBM cell line and healthy control pool using M-1, M-2, and SqEP method. Error bars are one standard deviation with n = 3. * p < 0.05, ** p <0.01, NS = not significant.

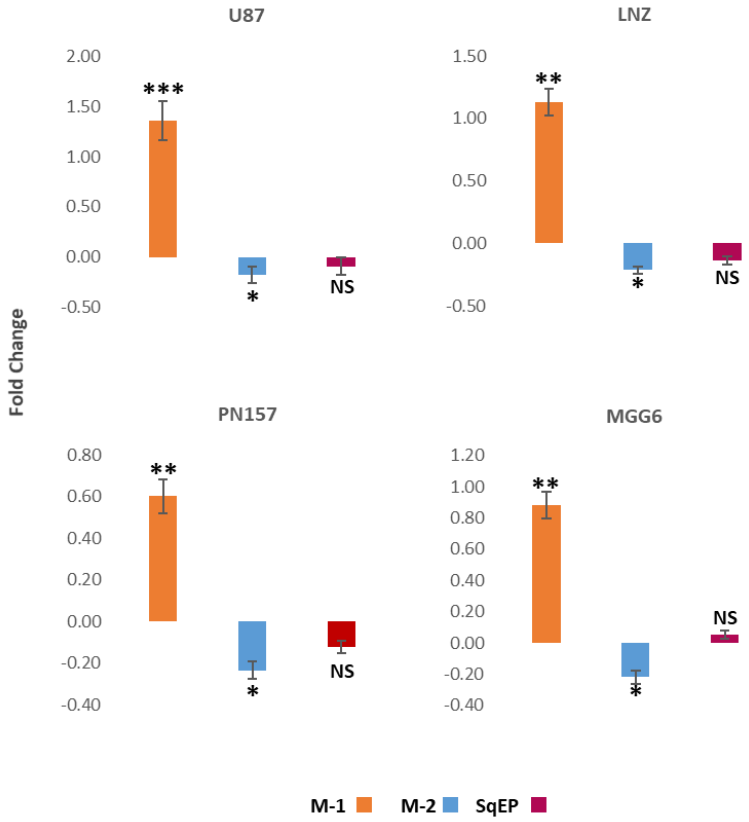

CHAPTER V: COMPARATIVE ANALYSIS OF GBM SENSITIVE TO TMZ VS RESISTANT

Introduction

Intratumoral heterogeneity in GBM is evidenced by the multiomic classification of GBM into classical, proneural, and mesenchymal subtypes. Each subtype is associated with variant disease progression or aggressiveness as well as treatment resistance[221]. Subtypes can transition throughout disease progression with the mesenchymal subtype being the most stable subtype following the tumor recurrence[222]. Glioblastoma stem cells are thought to be the source of tumor initiation and recurrence since GSCs maintain neural stem-like properties such as self-renewal and differentiation[223]. Proneural (PN) and mesenchymal (MES) are the two reported subtypes of GSCs. Consistent with differentiated tumor cells, GSCs also manifest differing sensitivities to clinical therapeutics [224,225]. MES GCSs are defined as the most aggressive and resistant subtype, thus the most lethal. Further, PN to MES GSC transitioning can occur by treatment with TMZ[52]. In this chapter the GBM RNA modification profile with and without drug resistance is compared. To mimic the phenotype and tumor heterogeneity, clinically relevant patient derived GSCs were used for in vitro analysis and in vivo implantation. The terms sensitive or resistant to treatment are assigned to PN and MES GSCs, respectively.

GBM in vitro analysis

The in vitro analysis of GBM with and without resistance to therapy will address the need to identify possible epitranscriptomic biomarkers for diagnostics or druggable targets. Glioma stem-like cells are grown and defined as sensitive or resistant to treatment by the previously described work of the Tannous Group [226,227]. Preclinical GBM models sensitive to TMZ include biological replicates (n=3) of low passage, serum free neurospheres MGG6, GBM8, and PN157. Preclinical GBM models resistant to TMZ include biological replicates (n=3) of low passage, serum free neurospheres MES 326, MES83, and MGG29. The samples were prepared and LC-

MS/MS analysis was performed as described in Chapters 2 and 4. Statistical analysis of normalized modified RNA (PCA, boxplots, and heatmaps) was executed in MetaboAnalyst[228].

In Chapter 3, a phenotypically repeatable GBM epitranscriptomic profile sensitive to TMZ was delineated. To address whether this profile is dysregulated in samples resistant to TMZ, the chemometrics analysis of the GBM epitranscriptome by principal component analysis (PCA) shows clustering of the two "phenotypes" with 95% confidence intervals indicated by elliptical shading (**Figure 23a**). Hierarchal clustering analysis also shows the grouping of samples by phenotypes of healthy, GBM sensitive, or GBM resistant (**Figure 23b**). Having identified the RNA modification profile to be unique between GBM with and without resistance to TMZ, we compared these changes quantitatively as indicated in the heatmap in **Figure 23b**. The top 3 significantly upregulated targets in the resistant GBM cells (m5C, t6A, and m6t6A) as compared to the sensitive GBM cells were identified by Log2 fold changes and two tailed student T test. Boxplots of the targets are shown in **Figure 24**. Each dot in a box plot represents the average of the biological replicates (n=3) in each represented GBM sample. The bottom and top of the

Figure 23. Qualitative and quantitative analysis of GBM in vitro. a). The relationship between GBM sensitive (pink) and GBM resistant (green) in vitro samples (n=3) is shown in PCA scores plot generated by MetaboAnalyst. Confidence intervals (95%) are indicated by colored ellipses. b) A clustering heatmap of GBM healthy control pool from donor RNA (green), GBM sensitive to TMZ (red), and GBM resistant to TMZ (blue).

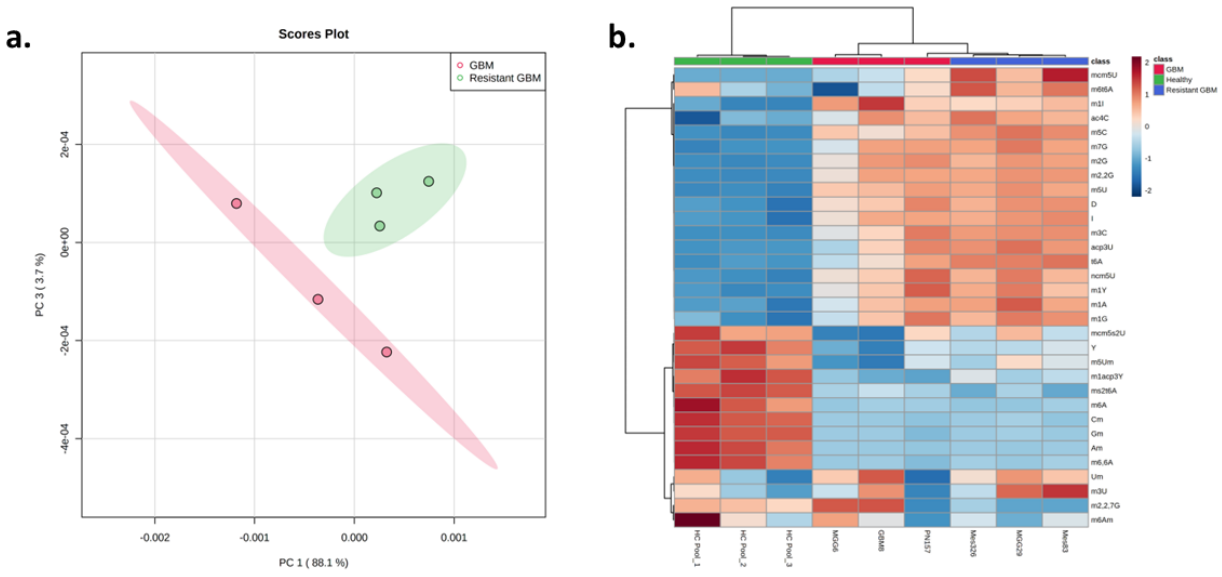

box represent the 25th and 75th or quartiles 1 and 3 (Q1 and Q3) respectively. The darkened band is the 50th percentile or Q2. The upper and lower whiskers indicate the maximum and minimum values.

Figure 24. The comparative abundance of the top 3 in vitro targets N6-threonylcarbamoyladenosine (t6A), N6-methyl-N6- threonylcarbamoyladenosine (m6t6A), and 5-methylcytidine (m5C) in GBM cells with and without TMZ resistance.

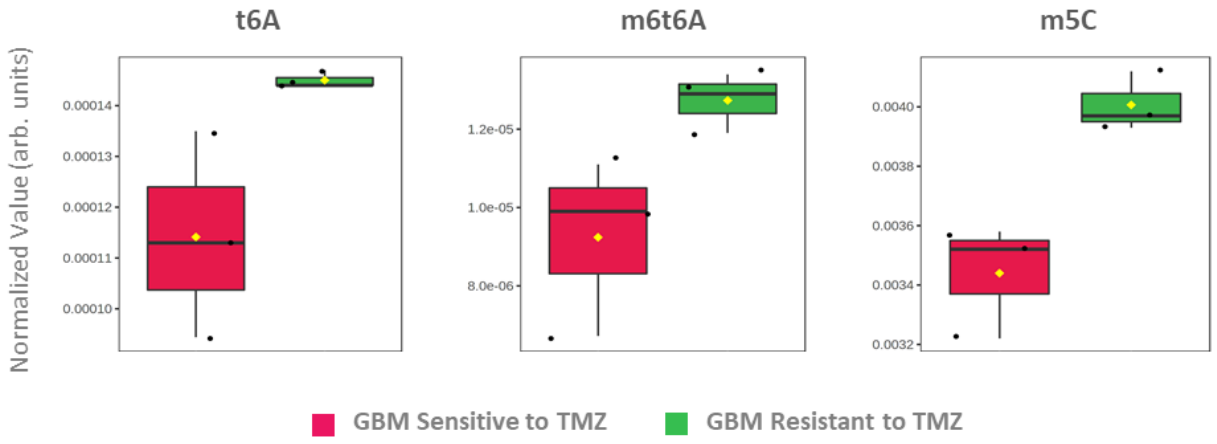

Preliminary GBM in vivo analysis

Following the elucidation of the RNA modification profile in GBM stem-like cells, an in vivo study considered the epitranscriptome of primary versus recurrent tumors. GBM8 cells engineered to express firefly luciferase (Fluc) and GFP fluorescent protein (Fluc-GFP) were intracranially injected in 16 weeks old female athymic mice. Briefly, mice were anesthetized with 3% isoflurane with oxygen and stereotactically injected (stereotactic coordinates: AP +0.5 / ML + 2.0 / DV -2.5 mm from Bregma) with 5 10^4 cells/2 μl in serum free culture medium using a 30-gauge Hamilton syringe. After tumor implantation mice were randomized into two groups primary tumor, which did not receive temozolomide (TMZ) treatment, and recurrent tumor, that received intraperitoneal injection of TMZ. Temozolomide treatment was performed in 2 different schedules: mice 1 received 5 mg/Kg TMZ for 2 days whereas mice 8 was treated with 5 mg/Kg for 2 days followed by 25 mg/Kg TMZ for 10 days (**Table 8**). The health status of the mice and

Table 8. GBM in vivo sample randomization with TMZ schedule and disclosure of poor body conditions (PBC).

Mouse ID	Tumor Type	TMZ Treatment	PBC (% mass loss)
1	recurrent	Y	20
8	recurrent	Y	20
3	primary	N	20
7	primary	N	18
9	primary	N	16

tumor growth were the criteria to determine the endpoint of the study (**Figure 25A-B**). Health status was determined by the assessment of pain signals, abnormal behavior, and body weight. Tumor growth was monitored by weekly bioluminescence imaging. TMZ treatment was initiated at week five when tumor signals were detected at 10-fold higher level than the background. All mouse studies were performed in accordance with the Massachusetts General Hospital

Figure 25. GBM8 cells expressing Fluc were intracranial injected in athymic mice, then health status and tumor growth were monitored over time. TMZ treatment was initiated when tumor signal was 10-fold higher than background. There is a direct association between mice body weight A) and tumor growth B), the bigger the tumor is, the worse the animal health status. It is relevant to notice that mice that received TMZ treatment exhibited tumor shrinkage and recovered body weight, which allowed them a longer survival.

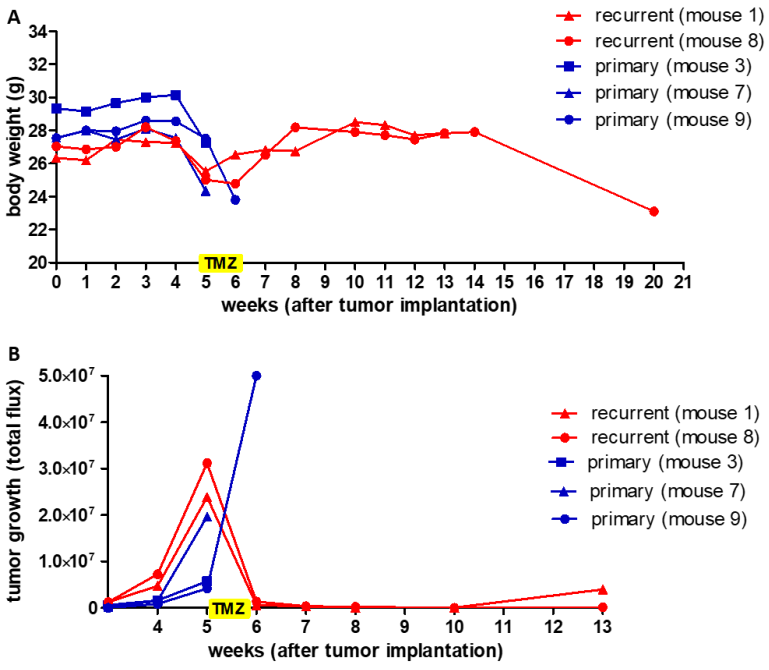

Subcommittee on Research Animal Care following guidelines set by the National Institutes of Health Guide for the Care and Use of Laboratory Animals.

During bioluminescence imaging, mice were injected intraperitoneally with 150 µg/g of D-luciferin and transferred into the Xenogen IVIS 200 Imaging System (PerkinElmer, Waltham, MA). Imaging was acquired 10 min post-luciferin injection and the image intensity was quantitated using the Living Image software 3.0 from Xenogen Imaging Technologies (PerkinElmer, Waltham, MA). Euthanasia was performed when mice showed concerned health status or tumor size. The brain was harvested, the tumor was dissected and washed in HBSS (Hank's Balanced Salt Saline), and immediately stored at -80^{o}C for further RNA purification.

Sample preparation, LC-MS/MS data acquisition, quantitation, chemometric and clustering analysis of the in vivo data set was performed as previously described. Having established the GBM RNA modification profile as distinct between those with and without resistance to TMZ in vitro, the PCA of GBM primary and recurrent tumors were plotted to assess if the pattern persists in vivo. The scores plot shows distinct grouping of the GBM primary and recurrent tumors within 95% confidence intervals (**Figure 26**). Hierarchical clustering analysis

Figure 26. PCA scores plot indicates grouping of samples by tumor type with GBM primary shown in red and GBM recurrent in green.

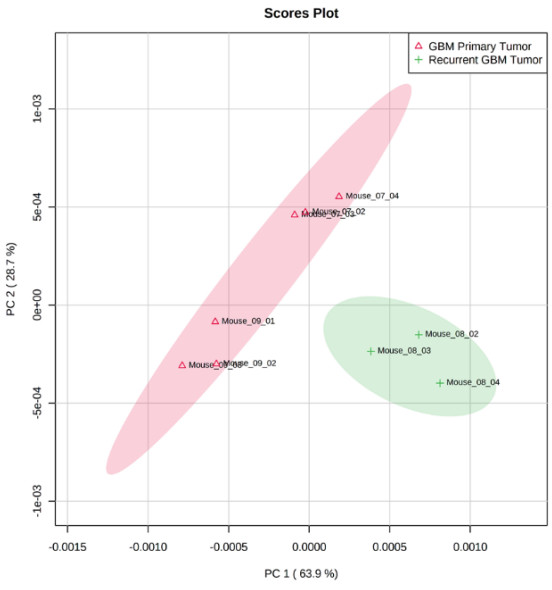

also groups the epitranscriptome of primary and recurrent GBM tumors distinctly. Following quantitation, the in vitro and in vivo analysis of the GBM epitranscriptome is comparable (**Figure 27A**). The dysregulation of the targets identified in vitro endure in the in vivo samples (**Figure 27B**). However, there are limitations to this data set that must be addressed. First and foremost, the sample size must be increased to ensure biological relevance and statistical significance. Secondly, the information gleaned from this experiment will allow for the optimization of criteria

Figure 27. Comparative analysis of the epitranscriptome in GBM primary and recurrent tumors in vivo. A). A heatmap with hierarchical analysis shows a comparative epitranscriptomic dysregulation by sample type to that found in GBM in vitro analysis. B). The upregulated targets identified in vitro (t6A, m6t6A, and m5C) persist in vivo.

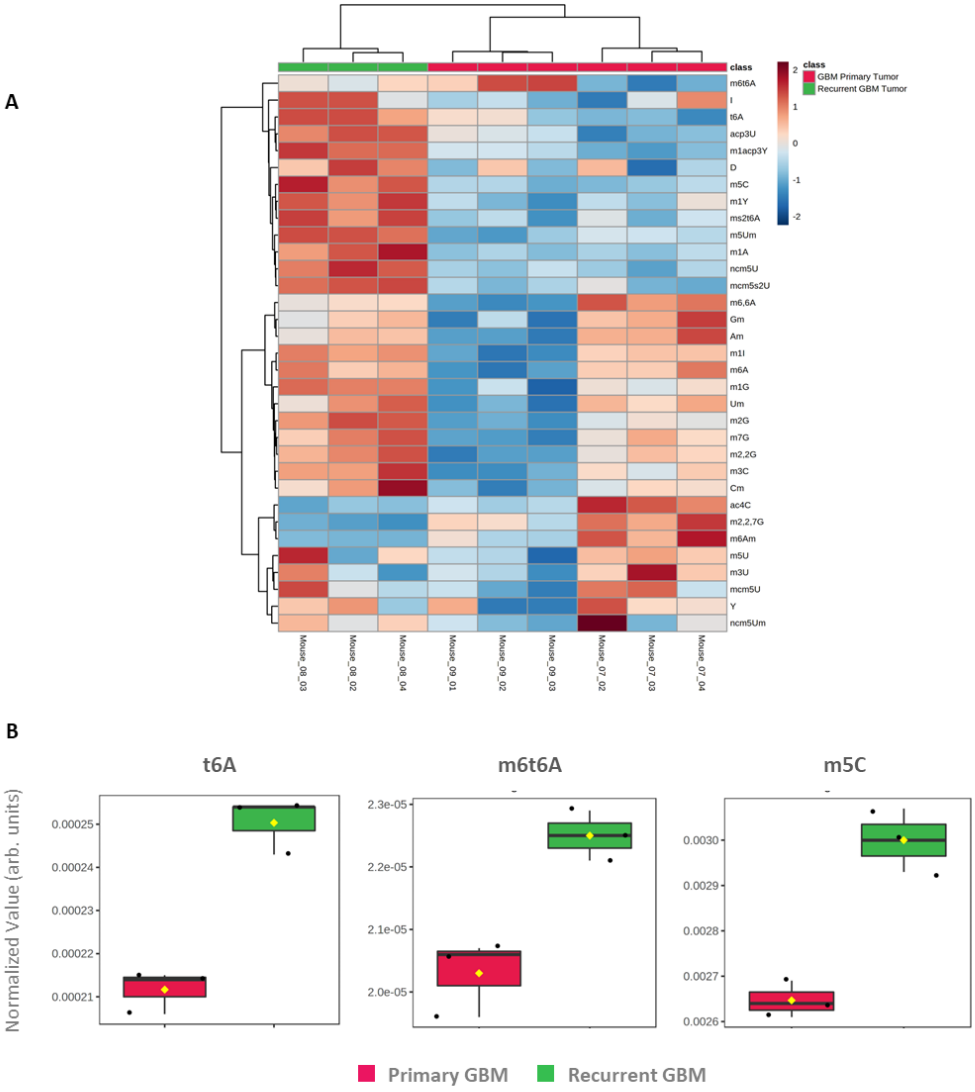

for the termination of the experiment. For example, there was no literature precedence for the mass of tumor needed to isolate sufficient RNA for LC-MS/MS analysis. A more specific bioluminescent signal target will ensure adequate tumor size without necrosis and unplanned loss of mice. Third, due to the sensitivity of the LC-MS/MS method it is critical to isolate the tumors without artifact tissue which can dilute the already low abundant targets (**Figure 28**)[229]. Thus, stereotatic coordinates are used only as a guide for more complete tumor dissection.

Figure 28. A representative extracted ion chromatogram (XIC) of the RNA modification m6t6A. Normal brain tissue from mouse 7 (black) and primary GBM sample from mouse 7 (red). All in vivo samples show a reduction of m6t6A in normal tissue which is also mirrored in the 5-person pool of RNA from donor brain tissue with no history of cancer used in the in vitro study. Total RNA artifacts from normal mouse tissue would dilute the level of the low abundant yet biologically relevant m6t6A in tumor samples.

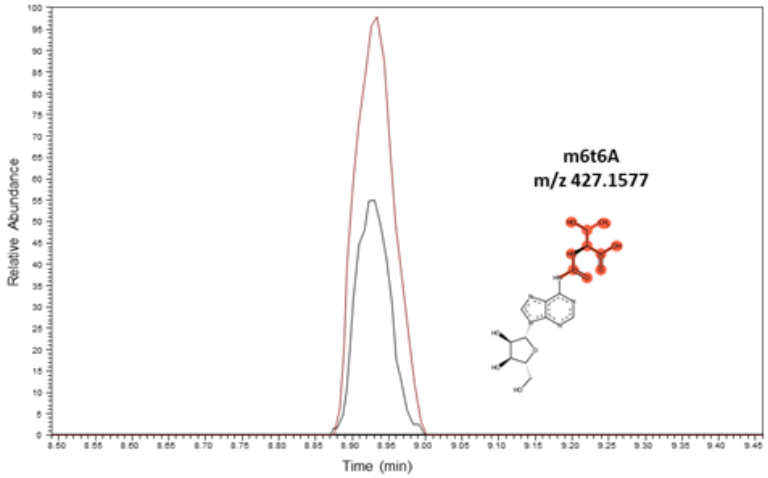

Preliminary Knockdown of TRMO in GBM resistant to TMZ

The analysis of the epitranscriptome in vitro (sensitive vs resistant GSC lines) and in vivo (primary vs recurrent tumor) demonstrated that the same set of RNA modification is upregulated in resistant GSC lines as well as in recurrent tumors. This suggests that the dysregulated RNA modifications could play a role in tumor resistance. Among all RNA modifications the three upregulated in resistant GSC lines and recurrent tumor identified as potential biomarker targets by our quantification method were t6A, m6t6A and m5C. The RNA modification, m6t6A, was selected as the primary target due to its specific location on tRNA and

unique writer enzyme[230]. To investigate the role of m6t6A in GBM resistance we knocked down its unique writer gene tRNA methyltransferase O (TRMO) and analyzed the impact upon TMZ sensitivity. The modification t6A and its writer gene O-Sialoglycoprotein endopeptidase (OSGEP) was not selected since t6A is the biosynthetic precursor to both m6t6A and ms2t6A in humans[231]. Though the writer for m5C originally identified by TCGA as biologically relevant, NSUN5, could be a potential target it is committed with important physiological pathways and knocking down its expression could lead to unwanted effects[232]. Also, the RNA modification m5C has multiple writers associated with it dependent upon the species of RNA it is located on.

Knocking down TRMO expression reduced cell viability (**Figure 29A-B**). There was no noted change to its morphology, but its growth rate was notably slowed which indicates that TRMO is essential to cellular activities (**Figure 30**). When the knockdowns were validated with LC-MS/MS, m6tA was present in the parent cell line while absent in all knockdown samples (**Figure 31**). Unexpectantly, all RNA modification levels were downregulated in the shTRMO

Figure 29. Knocking down TRMO expression in Mes326 cells compromise cell viability but did not affect cell sensitivity to DMSO. Increasing transducing units added to Mes326 cells led to a higher TRMO knock down efficiency (A). Knocking down TRMO expression resulted in reduction of cell viability (B). TRMO knock down efficiency is indirectly associated to cell viability. Interestingly, although knocking down TRMO expression reduced cell viability, it did not affect cells susceptibility to DMSO.

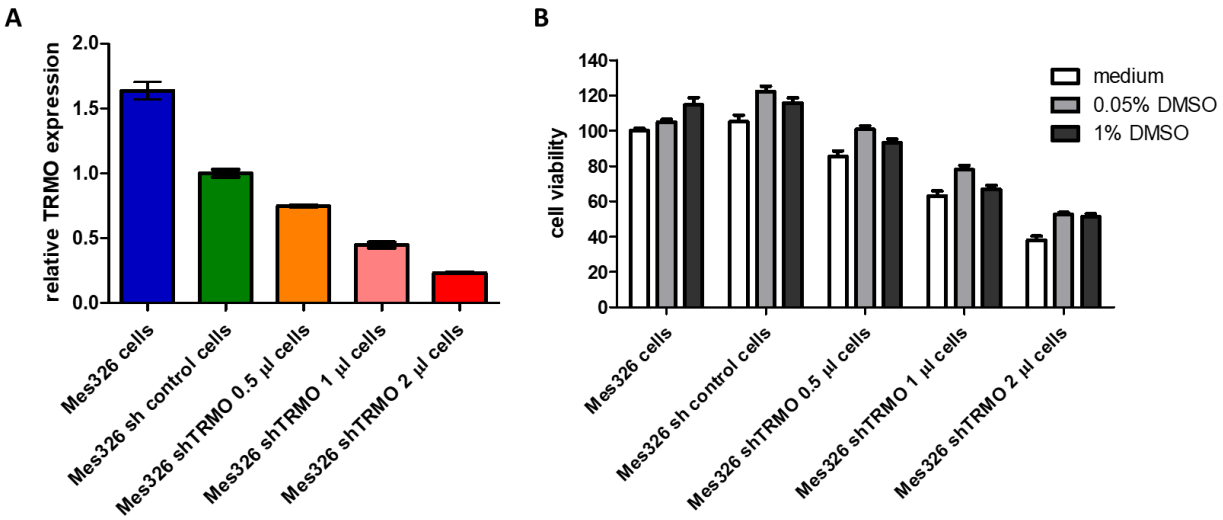

Figure 31. Microscopy image from Mes326 cells plain and knocked down to TRMO after 6 days in culture. Though knocking down TRMO expression reduced cell viability, it did not promote significant changes in cell morphology but neurospheres did grow significantly slower rate than plain Mes326 cells.

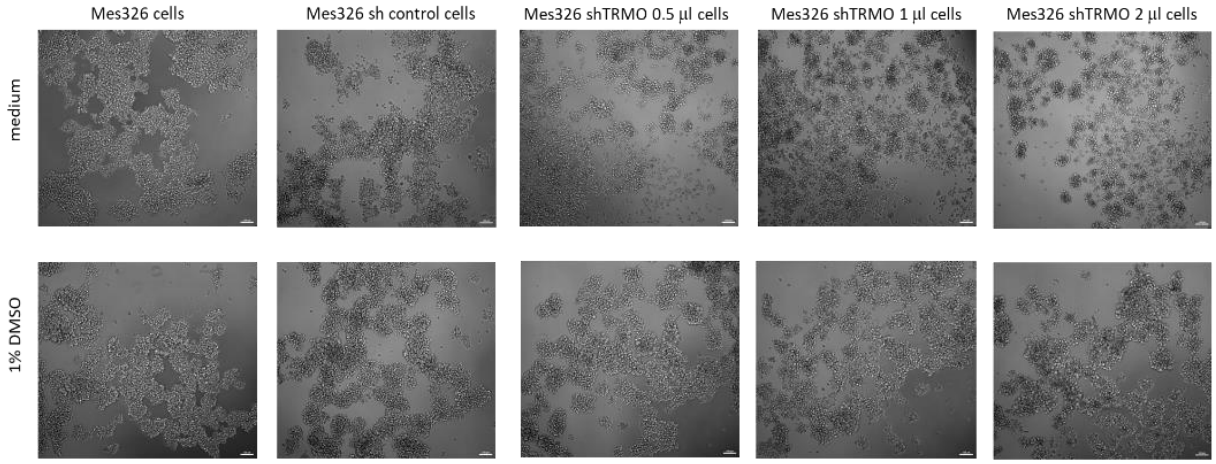

Figure 30. A representative XIC of the RNA modification m6t6A identified by m/z ± 5ppm, a retention time ± 0.1 min, and 2 MS^2 fragment ions. The modification was found in all resistant GBM cell lines (top chromatogram) and absent in all KDs (as seen in lower chromatogram).

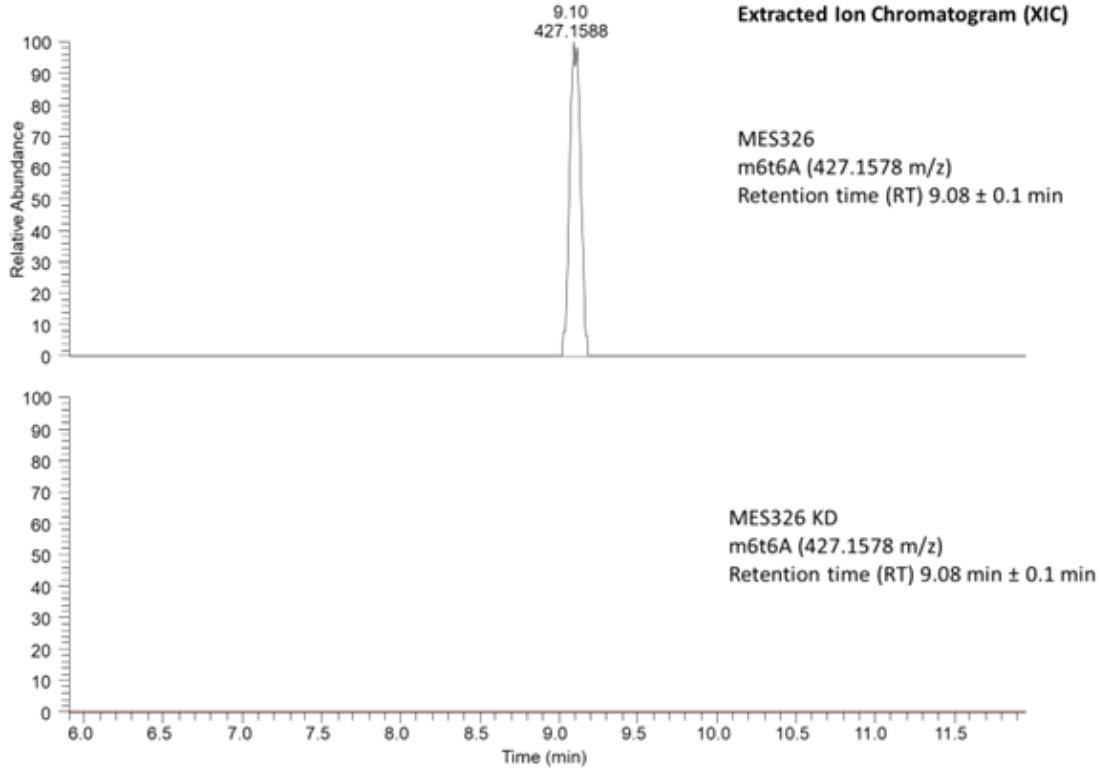

samples when compared to the parent cell line. Whether this is due to a reduction in cell proliferation or an increase in cell death needs to be addressed in future work. However, what is shown is that TRMO knockdown does promote a resensitization to TMZ as indicated by the IC50 curves in **Figure 32**. This could potentially lead to extended patient survival and should be explored for future clinical relevance.

Figure 32. TRMO expression knock down efficiency was > 85% in all resistant GSC lines analyzed by qRT-PCR. TRMO knockdown promoted TMZ sensitization in resistant GSC lines as noted by the induced shift to the left in TMZ dose curves in resistant GSC Mes83, MGG29, and Mes326.

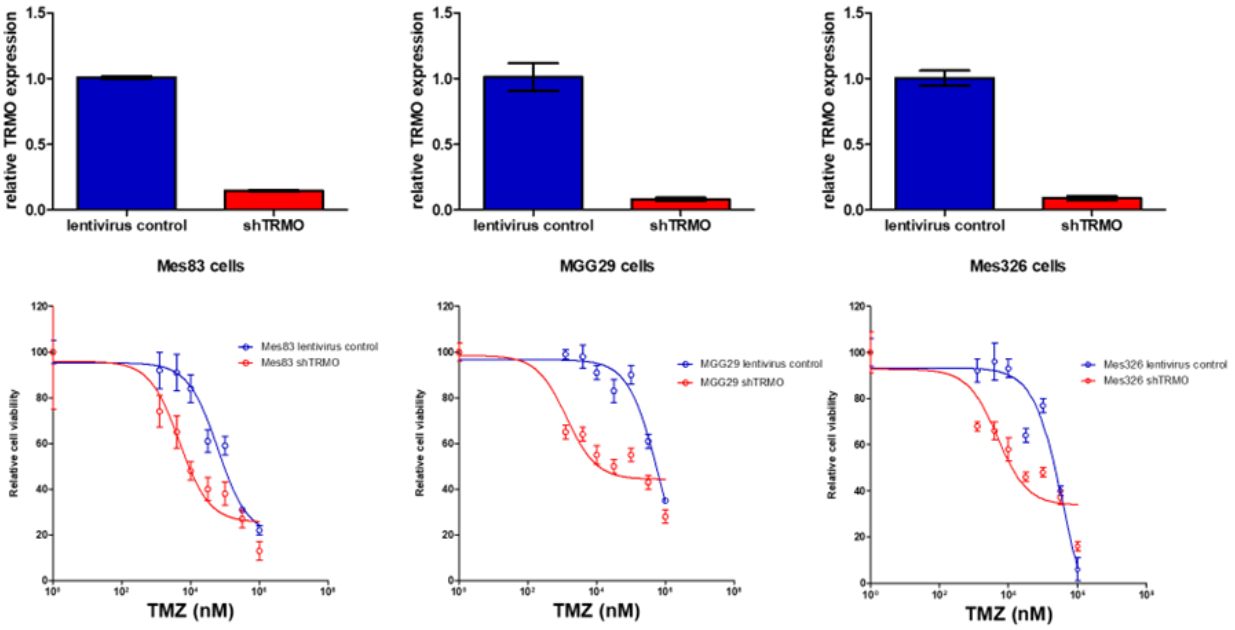

MGG29, Mes83 and Mes326 GSCs were derived from surgical specimens obtained from glioblastoma patients undergoing treatment, in accordance with the appropriate Institutional eview Board approval. GSCs were cultured as neurospheres in serum-free DMEM-F12 medium (Corning) supplemented with 2% B27 supplement (Gibco), 3mM GlutaMAX (Gibco), 20 ng/mL human recombinant EGF (abm) and 10 ηg/mL human recombinant bFGF-2 (abm).

GSCs were plated in six-well plates and infected with lentivirus vectors expressing shRNA against TRMO (Sigma, TRCN0000144999) or control lentivirus (expressing fluorescent

protein). Three days after virus infection, knockdown efficiency was assessed by qRT-PCR. Total RNA was isolated using Quick-RNA^{TM} Miniprep Kit (Zymo Research) following the instructions of the manufacturer. One microgram of total RNA was transcribed into cDNA using 5X All-In-One RT MasterMix cDNA synthesis kit (abm). qRT-PCR reaction was performed in QuantStudio 3 PCR system (Applied Biosystems) using SYBR Green Master Mix (Thermo Fisher) and primer pairs for TRMO (for, 5'-GCCAAGCTGGAAAAGGTAGAAGG-3'; rev, 5'-GGCTCCATCACATTTTGCGGTG-3') and GAPDH (For, 5`-GAAGGTGAAGGTCGGAGTCA-3`; rev, 5`-TTGAGGTCAATGAAGGGGTC-3`). GSCs previously infected with shRNA against TRMO (shTRMO) or control lentivirus were seeded in 96-well plates (3 x 10^3 cells/well), treated with indicated TMZ dose and cell viability was assessed 5 days later by alamarBlue assay (ThermoFisher) following manufacturers protocol.

Conclusion

In this chapter we consider the GBM epitranscriptomic profile with and without drug resistance in vitro and identify the target modifications t6A, m6t6A, and m5C to be upregulated in all MES GSC in vitro samples defined as resistant to TMZ. To further validate the biological relevance of these epitranscriptomic biomarkers a preclinical in vivo study was performed. Limitations with the study include small sample size and dilution of the total RNA by normal brain tissue artifacts. However, end of experiment determinants were optimized and early results support the in vitro model RNA modification targets of t6A, m6t6A, and m5C. This suggests that the dysregulated RNA modifications could play a role in tumor resistance.

If the modification does play a role in tumor resistance, then suppressing the writer for it should reduce the level of the modification and possibly resensitize the cells to treatment with TMZ. The RNA modification, m6t6A, was selected as the primary target for gene expression knockdown studies due to its specific location on tRNA and unique writer enzyme[230]. In all domains of life, t6A or derivatives have been reported at position 37 in tRNA which decode ANN codons (N = any nucleobase) and often regulate wobble-base pair interactions[233]. Kimura and

coworkers specify TRMO to discriminate for ACY codon[230]. A recent molecular dynamics simulation by Prabhakar et al. states that m6t6A can enhance base stacking in the anticodon loop which could lead to codon-biased translation[234]. The writer specificity of m6t6A potentiates it as a druggable target by a low molecular weight inhibitor of TRMO[235]. Even so, understanding the writer enzyme biochemistry and ligand binding pockets needs further elucidation for exploration in a clinical application.

The knockdown of TRMO in three resistant GSC lines reduced cell viability with no change to cellular morphology. Retarded cell growth upon gene suppression indicates that TRMO is essential to cellular functions and its dysregulation in resistant GSCs requires future work to uncover the associated mechanisms. Of most interest, however, is that upon knockdown of TRMO in MES326, MES83, and MGG29 the resistant GSCs shifted to a resensitized IC50 dosage. Just how the reduction of TRMO and subsequently m6t6A is resensitizing GBM to TMZ requires clarification. But resensitization to TMZ is a move in the right direction to increase the overall survival rate of patients diagnosed with GBM who are desperate for more time.

A better understanding into which RNA modifications are present and which are changing can enhance our understanding on the development of diseases. Most epitranscriptomic applications are limited to 1 of 7 modifications identified by NGS rather than system based empirically generated hypotheses. This work highlights the use of LC-MS/MS based epitranscriptomic profiling that can derive a posteriori hypothesis in a specific system accurately with up to 40 RNA modifications. While this project considered GBM with and without resistance to TMZ, it can translate to any system in any organism.

REFERENCES

1. Ostrom, Q. T. *et al.* CBTRUS Statistical Report: Primary Brain and Other Central Nervous System Tumors Diagnosed in the United States in 2013–2017. *Neuro-Oncology* **22**, iv1–iv96 (2020).
2. Perry, A. & Wesseling, P. Histologic classification of gliomas. *Handbook of Clinical Neurology* **134**, 71–95 (2016).
3. Tan, A. C. *et al.* Management of glioblastoma: State of the art and future directions. *CA: A Cancer Journal for Clinicians* **70**, 299–312 (2020).
4. Fernandes, C. *et al.* Current Standards of Care in Glioblastoma Therapy. *Exon Publications* 197–241 (2017) doi:10.15586/CODON.GLIOBLASTOMA.2017.CH11.
5. Brennan, C. W. *et al.* The Somatic Genomic Landscape of Glioblastoma. *Cell* **155**, 462–477 (2013).
6. McLendon, R. *et al.* Comprehensive genomic characterization defines human glioblastoma genes and core pathways. *Nature* **455**, 1061 (2008).
7. Verhaak, R. G. W. *et al.* Integrated Genomic Analysis Identifies Clinically Relevant Subtypes of Glioblastoma Characterized by Abnormalities in PDGFRA, IDH1, EGFR, and NF1. *Cancer Cell* **17**, 98–110 (2010).
8. Wang, Q. *et al.* Tumor Evolution of Glioma-Intrinsic Gene Expression Subtypes Associates with Immunological Changes in the Microenvironment. *Cancer Cell* **32**, 42-56.e6 (2017).
9. Sturm, D. *et al.* Hotspot Mutations in H3F3A and IDH1 Define Distinct Epigenetic and Biological Subgroups of Glioblastoma. *Cancer Cell* **22**, 425–437 (2012).
10. Phillips, H. S. *et al.* Molecular subclasses of high-grade glioma predict prognosis, delineate a pattern of disease progression, and resemble stages in neurogenesis. *Cancer Cell* **9**, 157–173 (2006).

11. Lee, E., Yong, R. L., Paddison, P. & Zhu, J. Comparison of glioblastoma (GBM) molecular classification methods. *Seminars in Cancer Biology* **53**, 201–211 (2018).

12. Azam, Z., Shing-Shun Tony, T. O. & Tannous, B. A. Mesenchymal Transformation: The Rosetta Stone of Glioblastoma Pathogenesis and Therapy Resistance. *Advanced Science* **7**, 2002015 (2020).

13. Shergalis, A., Bankhead, A., Luesakul, U., Muangsin, N. & Neamati, N. Current Challenges and Opportunities in Treating Glioblastoma. *Pharmacological Reviews* **70**, 412–445 (2018).

14. Becker, A. P., Sells, B. E., Jaharul Haque, S. & Chakravarti, A. Tumor Heterogeneity in Glioblastomas: From Light Microscopy to Molecular Pathology. *Cancers 2021, Vol. 13, Page 761* **13**, 761 (2021).

15. Parker, N. R., Khong, P., Parkinson, J. F., Howell, V. M. & Wheeler, H. R. Molecular heterogeneity in glioblastoma: Potential clinical implications. *Frontiers in Oncology* **5**, 55 (2015).

16. Patel, M., Mccully, C., Godwin, K. & Balis, F. M. *Plasma and cerebrospinal fluid pharmacokinetics of intravenous temozolomide in non-human primates*. *Journal of Neuro-Oncology* vol. 61 (2003).

17. Agarwala, S. S. & Kirkwood, J. M. Temozolomide, a Novel Alkylating Agent with Activity in the Central Nervous System, May Improve the Treatment of Advanced Metastatic Melanoma. *The Oncologist* **5**, 144–151 (2000).

18. Denny, B. J., Tsang, L. L. H., Slack, J. A., Wheelhouse, R. T. & Stevens, M. F. G. NMR and Molecular Modeling Investigation of the Mechanism of Activation of the Antitumor Drug Temozolomide and Its Interaction with DNA. *Biochemistry* **33**, 9045–9051 (1994).

19. Pegg, A. E., Dolan, M. E. & Moschel, R. C. Structure, Function, and Inhibition of O6-Alkylguanine-DNA Alkyltransferase. *Progress in Nucleic Acid Research and Molecular Biology* **51**, 167–223 (1995).

20. Mojas, N., Lopes, M. & Jiricny, J. Mismatch repair-dependent processing of methylation damage gives rise to persistent single-stranded gaps in newly replicated DNA. *Genes & Development* **21**, 3342 (2007).

21. Wedge, S. R. & Newlands, E. S. O6-benzylguanine enhances the sensitivity of a glioma xenograft with low O6-alkylguanine-DNA alkyltransferase activity to temozolomide and BCNU. *British Journal of Cancer 1996 73:9* **73**, 1049–1052 (1996).

22. Tisdale, M. J. Antitumour imidazotetrazines—XV: Role of guanine O6 alkylation in the mechanism of cytotoxicity of imidazotetrazinones. *Biochemical Pharmacology* **36**, 457–462 (1987).

23. Cejka, P. *et al.* Methylation-induced G(2)/M arrest requires a full complement of the mismatch repair protein hMLH1. *EMBO J* **22**, 2245–2254 (2003).

24. Patel, A. P. *et al.* Single-cell RNA-seq highlights intratumoral heterogeneity in primary glioblastoma. *Science* **344**, 1396 (2014).

25. Wang, J. *et al.* Clonal evolution of glioblastoma under therapy. *Nature Genetics 2016 48:7* **48**, 768–776 (2016).

26. Bhat, K. P. L. *et al.* Mesenchymal Differentiation Mediated by NF-κB Promotes Radiation Resistance in Glioblastoma. *Cancer Cell* **24**, 331–346 (2013).

27. da Hora, C. C. *et al.* Sustained NF-κB-STAT3 signaling promotes resistance to Smac mimetics in Glioma stem-like cells but creates a vulnerability to EZH2 inhibition. *Cell Death Discov* **5**, (2019).

28. Liu, T. *et al.* PDGF-mediated mesenchymal transformation renders endothelial resistance to anti-VEGF treatment in glioblastoma. *Nature Communications 2018 9:1* **9**, 1–13 (2018).

29. Teng, J. *et al.* Dissecting inherent intratumor heterogeneity in patient-derived glioblastoma culture models. *Neuro-Oncology* **19**, 820 (2017).

30. Mikheeva, S. A. *et al.* TWIST1 promotes invasion through mesenchymal change in human glioblastoma. *Molecular Cancer* **9**, 1–18 (2010).

31. Segerman, A. *et al.* Clonal Variation in Drug and Radiation Response among Glioma-Initiating Cells Is Linked to Proneural-Mesenchymal Transition. *Cell Reports* **17**, 2994–3009 (2016).

32. Takashima, Y., Kawaguchi, A. & Yamanaka, R. Promising Prognosis Marker Candidates on the Status of Epithelial–Mesenchymal Transition and Glioma Stem Cells in Glioblastoma. *Cells 2019, Vol. 8, Page 1312* **8**, 1312 (2019).

33. Halliday, J. *et al.* In vivo radiation response of proneural glioma characterized by protective p53 transcriptional program and proneural-mesenchymal shift. *Proc Natl Acad Sci U S A* **111**, 5248–5253 (2014).

34. Carro, M. S. *et al.* The transcriptional network for mesenchymal transformation of brain tumors. *Nature* **463**, 318 (2010).

35. Minata, M. *et al.* Phenotypic Plasticity of Invasive Edge Glioma Stem-like Cells in Response to Ionizing Radiation. *Cell Reports* **26**, 1893-1905.e7 (2019).

36. Fedele, M., Cerchia, L., Pegoraro, S., Sgarra, R. & Manfioletti, G. Proneural-Mesenchymal Transition: Phenotypic Plasticity to Acquire Multitherapy Resistance in Glioblastoma. *International Journal of Molecular Sciences 2019, Vol. 20, Page 2746* **20**, 2746 (2019).

37. Li, J. *et al.* The role of mRNA m 6 A methylation in the nervous system. doi:10.1186/s13578-019-0330-y.

38. Abels, E. R. *et al.* Glioblastoma-Associated Microglia Reprogramming Is Mediated by Functional Transfer of Extracellular miR-21. *Cell Reports* **28**, 3105-3119.e7 (2019).

39. Broekman, M. L. *et al.* Multidimensional communication in the microenvirons of glioblastoma. *Nat Rev Neurol* **14**, 482 (2018).

40. Schweiger, M. W. *et al.* Extracellular Vesicles Induce Mesenchymal Transition and Therapeutic Resistance in Glioblastomas through NF-κB/STAT3 Signaling. *Advanced Biosystems* **4**, 1900312 (2020).

41. Zheng, X. *et al.* Epithelial-to-mesenchymal transition is dispensable for metastasis but induces chemoresistance in pancreatic cancer. *Nature 2015 527:7579* **527**, 525–530 (2015).

42. Fischer, K. R. *et al.* Epithelial-to-mesenchymal transition is not required for lung metastasis but contributes to chemoresistance. *Nature 2015 527:7579* **527**, 472–476 (2015).

43. Sánchez-Tilló, E. *et al.* EMT-activating transcription factors in cancer: beyond EMT and tumor invasiveness. *Cellular and Molecular Life Sciences 2012 69:20* **69**, 3429–3456 (2012).

44. Kalluri, R. & Weinberg, R. A. The basics of epithelial-mesenchymal transition. *The Journal of Clinical Investigation* **119**, 1420–1428 (2009).

45. Smith, B. N., Bhowmick, N. A., Brenner, D. A., Kisseleva, T. & Fuxe, J. Role of EMT in Metastasis and Therapy Resistance. *Journal of Clinical Medicine 2016, Vol. 5, Page 17* **5**, 17 (2016).

46. Parker, N. R., Khong, P., Parkinson, J. F., Howell, V. M. & Wheeler, H. R. Molecular heterogeneity in glioblastoma: Potential clinical implications. *Frontiers in Oncology* **5**, 55 (2015).

47. Qazi, M. A. *et al.* Intratumoral heterogeneity: pathways to treatment resistance and relapse in human glioblastoma. *Annals of Oncology* **28**, 1448–1456 (2017).

48. Clarke, M. F. *et al.* Cancer stem cells - Perspectives on current status and future directions: AACR workshop on cancer stem cells. *Cancer Research* **66**, 9339–9344 (2006).

49. Chen, J. *et al.* A restricted cell population propagates glioblastoma growth after chemotherapy. *Nature 2012 488:7412* **488**, 522–526 (2012).

50. Eyler, C. E. & Rich, J. N. Survival of the Fittest: Cancer Stem Cells in Therapeutic Resistance and Angiogenesis. *J Clin Oncol* **26**, 2839 (2008).

51. Bao, S. *et al.* Glioma stem cells promote radioresistance by preferential activation of the DNA damage response. *Nature 2006 444:7120* **444**, 756–760 (2006).

52. Wang, Z., Zhang, H., Xu, S., Liu, Z. & Cheng, Q. The adaptive transition of glioblastoma stem cells and its implications on treatments. *Signal Transduction and Targeted Therapy 2021 6:1* **6**, 1–13 (2021).

53. Chen, X. *et al.* A novel enhancer regulates MGMT expression and promotes temozolomide resistance in glioblastoma. *Nature Communications* **9**, 2949 (2018).

54. Kitange, G. J. *et al.* Induction of MGMT expression is associated with temozolomide resistance in glioblastoma xenografts. *Neuro-Oncology* **11**, 281 (2009).

55. Yip, S. *et al.* MSH6 mutations arise in glioblastomas during temozolomide therapy and mediate temozolomide resistance. *Clinical Cancer Research* **15**, 4622–4629 (2009).

56. Mismatch Repair Mutations Override Alkyltransferase in Conferring Resistance to Temozolomide but not to 1,3-Bis(2-chloroethyl)nitrosourea1 | Cancer Research | American Association for Cancer Research. https://aacrjournals.org/cancerres/article/56/23/5375/502732/Mismatch-Repair-Mutations-Override.

57. Yoshimoto, K. *et al.* Complex DNA repair pathways as possible therapeutic targets to overcome temozolomide resistance in glioblastoma. *Frontiers in Oncology* **0**, 186 (2012).

58. Serrano-Heras, G. *et al.* Involvement of N-methylpurine DNA glycosylase in resistance to temozolomide in patient-derived glioma cells. doi:10.1038/s41598-020-78868-0.

59. Banelli, B. *et al.* Review Article MicroRNA in Glioblastoma: An Overview. (2017) doi:10.1155/2017/7639084.

60. Peng, Y. & Croce, C. M. The role of MicroRNAs in human cancer. (2016) doi:10.1038/sigtrans.2015.4.

61. Chan, J. A., Krichevsky, A. M. & Kosik, K. S. MicroRNA-21 Is an Antiapoptotic Factor in Human Glioblastoma Cells. *Cancer Research* **65**, 6029–6033 (2005).

62. MicroRNA-21 Inhibition Enhances In Vitro Chemosensitivity.

63. Teplyuk, N. M. *et al.* Therapeutic potential of targeting microRNA-10b in established intracranial glioblastoma: first steps toward the clinic. *EMBO Molecular Medicine* **8**, 268–287 (2016).

64. Shi, L. *et al.* MiR-21 protected human glioblastoma U87MG cells from chemotherapeutic drug temozolomide induced apoptosis by decreasing Bax/Bcl-2 ratio and caspase-3 activity. *Brain Research* **1352**, 255–264 (2010).

65. Fu, Z. & Tindall, D. J. FOXOs, cancer and regulation of apoptosis. *Oncogene* **27**, 2312 (2008).

66. Strik, H. *et al.* BCL-2 Family protein expression in initial and recurrent glioblastomas: modulation by radiochemotherapy. doi:10.1136/jnnp.67.6.763.

67. Foster, K. A., Jane, E. P., Premkumar, D. R., Morales, A. & Pollack, I. F. Co-administration of ABT-737 and SAHA induces apoptosis, mediated by Noxa upregulation, Bax activation and mitochondrial dysfunction in PTEN-intact malignant human glioma cell lines. doi:10.1007/s11060-014-1575-2.

68. Berghauser Pont, L. M. E. *et al.* The Bcl-2 inhibitor Obatoclax overcomes resistance to histone deacetylase inhibitors SAHA and LBH589 as radiosensitizers in patient-derived glioblastoma stem-like cells. *Genes & Cancer* **5**, 445 (2014).

69. Katayama, M., Kawaguchi, T., Berger, M. S. & Pieper, R. O. DNA damaging agent-induced autophagy produces a cytoprotective adenosine triphosphate surge in malignant glioma cells. *Cell Death & Differentiation 2007 14:3* **14**, 548–558 (2006).

70. Karmur, B. S. *et al.* Blood-Brain Barrier Disruption in Neuro-Oncology: Strategies, Failures, and Challenges to Overcome. *Frontiers in Oncology* **10**, 1811 (2020).

71. Cardoso, F. L., Brites, D. & Brito, M. A. Looking at the blood–brain barrier: Molecular anatomy and possible investigation approaches. *Brain Research Reviews* **64**, 328–363 (2010).

72. Munoz, J. L., Walker, N. D., Scotto, K. W. & Rameshwar, P. Temozolomide competes for P-glycoprotein and contributes to chemoresistance in glioblastoma cells. *Cancer Letters* **367**, 69–75 (2015).

73. Noch, E. K., Ramakrishna, R. & Magge, R. Challenges in the Treatment of Glioblastoma: Multisystem Mechanisms of Therapeutic Resistance. *World Neurosurgery* **116**, 505–517 (2018).

74. de Gooijer, M. C. *et al.* ATP-binding cassette transporters restrict drug delivery and efficacy against brain tumors even when blood-brain barrier integrity is lost. *Cell Reports Medicine* **2**, 100184 (2021).

75. Griffith, J. I., Sarkaria, J. N. & Elmquist, W. F. Efflux Limits Tumor Drug Delivery Despite Disrupted BBB. *Trends in Pharmacological Sciences* **42**, 426–428 (2021).

76. Davis, F. Ribonucleic Acids from Yeast Which Contain a Fifth Nucleotide.

77. Boccaletto, P. *et al.* MODOMICS: A database of RNA modification pathways. 2017 update. *Nucleic Acids Research* **46**, D303–D307 (2018).

78. Zhou, Y. *et al.* Principles of RNA methylation and their implications for biology and medicine. *Biomedicine & Pharmacotherapy* **131**, 110731 (2020).

79. Yablonovitch, A. L., Deng, P., Jacobson, D. & Li, J. B. The evolution and adaptation of A-to-I RNA editing. (2017) doi:10.1371/journal.pgen.1007064.

80. Nachtergaele, S. & He, C. Chemical Modifications in the Life of an mRNA Transcript. *https://doi.org/10.1146/annurev-genet-120417-031522* **52**, 349–372 (2018).

81. Jia, G. *et al.* N6-Methyladenosine in nuclear RNA is a major substrate of the obesity-associated FTO. *Nature Chemical Biology* (2011) doi:10.1038/nchembio.687.

82. Mauer, J. *et al.* Reversible methylation of m6Am in the 5′ cap controls mRNA stability. *Nature* **541**, 371 (2017).

83. Meyer, K. D. & Jaffrey, S. R. Rethinking m6A Readers, Writers, and Erasers. *https://doi.org/10.1146/annurev-cellbio-100616-060758* **33**, 319–342 (2017).

84. Fu, Y., Dominissini, D., Rechavi, G. & He, C. Gene expression regulation mediated through reversible m 6 A RNA methylation. *Nature Reviews Genetics* vol. 15 293–306 (2014).

85. Simen Zhao, B., Nachtergaele, S. & Roundtree, I. A. Our views of dynamic N 6-methyladenosine RNA methylation. (2018) doi:10.1261/rna.

86. Mauer, J., Jaffrey, S. R. & Jaffrey, S. R. FTO, m 6 A m , and the hypothesis of reversible epitranscriptomic mRNA modifications. doi:10.1002/1873-3468.13092.

87. Darnell, R. R., Shengdong, K. E. & Darnell, J. E. Pre-mRNA processing includes N6 methylation of adenosine residues that are retained in mRNA exons and the fallacy of "RNA epigenetics." *RNA* **24**, 262–267 (2018).

88. Chiu, N. H. L., Simpson, J. H., Wang, H. & Tannous, B. A. A theoretical perspective of the physical properties of different RNA modifications with respect to RNA duplexes. *BBA Advances* **1**, 100025 (2021).

89. Schimmel, P. Parameters for the molecular recognition of transfer RNAs. *Biochemistry* **28**, 2747–2759 (1989).

90. Sloan, K. E. *et al.* Tuning the ribosome: The influence of rRNA modification on eukaryotic ribosome biogenesis and function. *RNA Biology* vol. 14 1138–1152 (2017).

91. Roundtree, I. A., Evans, M. E., Pan, T. & He, C. Dynamic RNA Modifications in Gene Expression Regulation. *Cell* **169**, 1187–1200 (2017).

92. de Paolis, V. *et al.* cancers Epitranscriptomics: A New Layer of microRNA Regulation in Cancer. (2021) doi:10.3390/cancers13133372.

93. Jonkhout, N. *et al.* The RNA modification landscape in human disease. *Rna* **23**, 1754–1769 (2017).

94. Esteve-Puig, R., Bueno-Costa, A. & Esteller, M. Writers, readers and erasers of RNA modifications in cancer. *Cancer Letters* vol. 474 127–137 (2020).

95. Barbieri, I. & Kouzarides, T. Role of RNA modifications in cancer. *Nature Reviews Cancer* **20**, 303–322 (2020).

96. Visvanathan, A. *et al.* Essential role of METTL3-mediated m 6 A modification in glioma stem-like cells maintenance and radioresistance. *Oncogene* **37**, 522–533 (2018).

97. Wang, W., Li, J., Lin, F., Guo, J. & Zhao, J. Identification of N 6-methyladenosine-related lncRNAs for patients with primary glioblastoma. doi:10.1007/s10143-020-01238-x.

98. Cui, Q. *et al.* m6A RNA Methylation Regulates the Self-Renewal and Tumorigenesis of Glioblastoma Stem Cells. *Cell Reports* **18**, 2622–2634 (2017).

99. Li, F., Zhang, C. & Zhang, G. m6A RNA Methylation Controls Proliferation of Human Glioma Cells by Influencing Cell Apoptosis. *Cytogenetic and Genome Research* **159**, 119–125 (2019).

100. Xi, Z. *et al. Overexpression of miR-29a reduces the oncogenic properties of glioblastoma stem cells by downregulating Quaking gene isoform 6*. www.impactjournals.com/oncotarget.

101. Jin, D.-I. *et al.* Expression and roles of Wilms' tumor 1-associating protein in glioblastoma. (2012) doi:10.1111/cas.12022.

102. Xi, Z. *et al.* WTAP Expression Predicts Poor Prognosis in Malignant Glioma Patients. (2031) doi:10.1007/s12031-016-0788-6.

103. Hatanpaa, K. J., Burma, S., Zhao, D. & Habib, A. A. Epidermal Growth Factor Receptor in Glioma: Signal Transduction, Neuropathology, Imaging, and Radioresistance. *Neoplasia* **12**, 675 (2010).

104. Ping, X.-L. *et al.* Mammalian WTAP is a regulatory subunit of the RNA N6-methyladenosine methyltransferase. *Cell Research* **24**, 177–189 (2014).

105. Selberg, S. *et al.* Discovery of Small Molecules that Activate RNA Methylation through Cooperative Binding to the METTL3-14-WTAP Complex Active Site. (2019) doi:10.1016/j.celrep.2019.02.100.

106. Zhang, S. *et al.* m6A Demethylase ALKBH5 Maintains Tumorigenicity of Glioblastoma Stem-like Cells by Sustaining FOXM1 Expression and Cell Proliferation Program. *Cancer Cell* **31**, 591-606.e6 (2017).

107. Dong, Z. & Cui, H. The Emerging Roles of RNA Modifications in Glioblastoma. *Cancers 2020, Vol. 12, Page 736* **12**, 736 (2020).

108. Zhu, S. *et al.* An oncopeptide regulates m 6 A recognition by the m 6 A reader IGF2BP1 and tumorigenesis. doi:10.1038/s41467-020-15403-9.

109. Zhang, Y. *et al.* m6A modification in RNA: biogenesis, functions and roles in gliomas. *Journal of Experimental & Clinical Cancer Research 2020 39:1* **39**, 1–16 (2020).

110. Tuncel, G. & Kalkan, R. Importance of m N 6-methyladenosine (m 6 A) RNA modification in cancer. *Medical Oncology* **36**, 36 (2032).

111. Liu, Z. X., Li, L. M., Sun, H. L. & Liu, S. M. Link Between m6A Modification and Cancers. *Frontiers in Bioengineering and Biotechnology* **6**, 89 (2018).

112. Cheng, S.-Y. *et al.* The Roles and Regulation of m 6 A Modification in Glioblastoma Stem Cells and Tumorigenesis. (2022) doi:10.3390/biomedicines10050969.

113. Galardi, S., Michienzi, A. & Ciafrè, S. A. Insights into the Regulatory Role of m6A Epitranscriptome in Glioblastoma. *International Journal of Molecular Sciences 2020, Vol. 21, Page 2816* **21**, 2816 (2020).

114. Orellana, E. A. *et al.* METTL1-mediated m7G modification of Arg-TCT tRNA drives oncogenic transformation. *Molecular Cell* **81**, 3323-3338.e14 (2021).

115. Besse, A. *et al.* MiR-338-5p sensitizes glioblastoma cells to radiation through regulation of genes involved in DNA damage response. doi:10.1007/s13277-015-4654-x.

116. Chiu, Y. C., Hsiao, T. H., Chen, Y. & Chuang, E. Y. Parameter optimization for constructing competing endogenous RNA regulatory network in glioblastoma multiforme and other cancers. *BMC Genomics* **16**, 1–13 (2015).

117. Zhao, Y. *et al.* m1A Regulated Genes Modulate PI3K/AKT/mTOR and ErbB Pathways in Gastrointestinal Cancer. *Translational Oncology* **12**, 1323–1333 (2019).

118. Macari, F. *et al.* TRM6/61 connects PKCα with translational control through tRNAiMet stabilization: impact on tumorigenesis. *Oncogene 2016 35:14* **35**, 1785–1796 (2015).

119. Wang, Y., Huang, Q., Deng, T., Li, B. H. & Ren, X. Q. Clinical Significance of TRMT6 in Hepatocellular Carcinoma: A Bioinformatics-Based Study. *Medical Science Monitor : International Medical Journal of Experimental and Clinical Research* **25**, 3894 (2019).

120. Kim, Y.-W. *et al.* Identification of prognostic gene signatures of glioblastoma: a study based on TCGA data analysis. doi:10.1093/neuonc/not024.

121. Wang, P. *et al.* Identification of RNA: 5-Methylcytosine Methyltransferases-Related Signature for Predicting Prognosis in Glioma. *Frontiers in Oncology* **10**, (2020).

122. Janin, M. *et al.* Epigenetic loss of RNA-methyltransferase NSUN5 in glioma targets ribosomes to drive a stress adaptive translational program. *Acta Neuropathologica* **138**, 1053 (2019).

123. Zhou, J. *et al.* 61 Functional characterization of ribosomal RNA methyltransferase NSUN5 in glioblastoma. *Canadian Journal of Neurological Sciences* **45**, S10–S11 (2018).

124. Bhawe, K. *et al.* Nuclear Respiratory Factor 1 (NRF1) Transcriptional Activity-Driven Gene Signature Association with Severity of Astrocytoma and Poor Prognosis of Glioblastoma. *Molecular Neurobiology* **57**, 3827–3845 (2020).

125. Awah, C. U., Winter, J., Mazdoom, C. M. & Ogunwobi, O. O. NSUN6, an RNA methyltransferase of 5-mC controls glioblastoma response to temozolomide (TMZ) via NELFB and RPS6KB2 interaction. (2021) doi:10.1080/15384047.2021.1990631.

126. Wang, J. *et al.* ALYREF Drives Cancer Cell Proliferation Through an ALYREF-MYC Positive Feedback Loop in Glioblastoma. (2021) doi:10.2147/OTT.S286408.

127. Li, X., Ma, S. & Yi, C. Pseudouridine: the fifth RNA nucleotide with renewed interests. *Current Opinion in Chemical Biology* **33**, 108–116 (2016).

128. Cui, Q. *et al.* Targeting PUS7 suppresses tRNA pseudouridylation and glioblastoma tumorigenesis. *Nat Cancer* **2**, 932 (2021).

129. Zhang, D. Y., Ming, G.-L. & Song, H. PUS7: a targetable epitranscriptomic regulator of glioblastoma growth. (2021) doi:10.1016/j.tips.2021.10.002.

130. Wang, L. J., Lv, P., Lou, Y. & Ye, J. Gene Expression-Based Predication of RNA Pseudouridine Modification in Tumor Microenvironment and Prognosis of Glioma Patients. *Frontiers in Cell and Developmental Biology* **9**, 3865 (2022).

131. Srinivasan, S., Torres, A. G., Ribas De Pouplana, L., Alexander, R. W. & Hendrickson, T. L. Inosine in Biology and Disease. (2021) doi:10.3390/genes12040600.

132. Paz, N. *et al.* Altered adenosine-to-inosine RNA editing in human cancer. *Genome Research* **17**, 1586–1595 (2007).

133. Choudhury, Y. *et al.* Attenuated adenosine-to-inosine editing of microRNA-376a*promotes invasiveness of glioblastoma cells. *Journal of Clinical Investigation* **122**, 4059–4076 (2012).

134. Tassinari, V. *et al.* ADAR1 is a new target of METTL3 and plays a pro-oncogenic role in glioblastoma by an editing-independent mechanism. doi:10.1186/s13059-021-02271-9.

135. Xu, J. *et al.* The Non-N6-Methyladenosine Epitranscriptome Patterns and Characteristics of Tumor Microenvironment Infiltration and Mesenchymal Transition in Glioblastoma. *Frontiers in Immunology* **12**, (2022).

136. Peer, E., Rechavi, G. & Dominissini, D. Epitranscriptomics: regulation of mRNA metabolism through modifications. *Current Opinion in Chemical Biology* **41**, 93–98 (2017).

137. Motorin, Y. & Helm, M. RNA nucleotide methylation: 2021 update. *Wiley Interdisciplinary Reviews: RNA* **13**, (2022).

138. Motorin, Y. & Helm, M. Methods for RNA modification mapping using deep sequencing: Established and new emerging technologies. *Genes (Basel)* **10**, (2019).

139. Motorin, Y. & Helm, M. Methods for RNA Modification Mapping Using Deep Sequencing: Established and New Emerging Technologies. doi:10.3390/genes10010035.

140. Grozhik, A. v. & Jaffrey, S. R. Distinguishing RNA modifications from noise in epitranscriptome maps. *Nature Chemical Biology* vol. 14 215–225 (2018).

141. Grozhik, A. v. & Jaffrey, S. R. Epitranscriptomics: Shrinking maps of RNA modifications. *Nature* **551**, 174–176 (2017).

142. Sas-Chen, A. & Schwartz, S. Misincorporation signatures for detecting modifications in mRNA: Not as simple as it sounds. *Methods* **156**, 53–59 (2019).

143. Xiong, X., Li, X., Wang, K. & Yi, C. Perspectives on topology of the human m 1 A methylome at single nucleotide resolution. *RNA* **24**, 1437–1442 (2018).

144. Schwartz, S. M 1 A within cytoplasmic mRNAs at single nucleotide resolution: A reconciled transcriptome-wide map. *RNA* **24**, 1427–1436 (2018).

145. Grozhik, A. v. *et al.* Antibody cross-reactivity accounts for widespread appearance of m1A in 5'UTRs. *Nature Communications 2019 10:1* **10**, 1–13 (2019).

146. Helm, M., Lyko, F. & Motorin, Y. Limited antibody specificity compromises epitranscriptomic analyses. *Nature Communications 2019 10:1* **10**, 1–3 (2019).

147. Sarkar, A. *et al.* Detecting the epitranscriptome. *Wiley Interdisciplinary Reviews: RNA* **12**, e1663 (2021).

148. Liu, L. *et al.* Bioinformatics approaches for deciphering the epitranscriptome: Recent progress and emerging topics. *Computational and Structural Biotechnology Journal* **18**, 1587–1604 (2020).

149. Xie, S. *et al.* Applications and potentials of nanopore sequencing in the (epi)genome and (epi)transcriptome era. *The Innovation* **2**, 100153 (2021).

150. Moshitch-Moshkovitz, S., Dominissini, D. & Rechavi, G. The epitranscriptome toolbox. *Cell* **185**, 764–776 (2022).

151. Alfonzo, J. D. *et al. A call for direct sequencing of full-length RNAs to identify all modifications*. www.nature.com/naturegenetics doi:10.1038/s41588-021-00903-1.

152. Stephenson, W. *et al.* Direct detection of RNA modifications and structure using single-molecule nanopore sequencing. *Cell Genomics* **2**, 100097 (2022).

153. Wang, Y., Zhao, Y. & Bollas, A. ✉. Nanopore sequencing technology, bioinformatics and applications. doi:10.1038/s41587-021-01108-x.

154. Motorin, Y. & Helm, M. Methods for RNA Modification Mapping Using Deep Sequencing: Established and New Emerging Technologies. doi:10.3390/genes10010035.

155. Motorin, Y. & Marchand, V. Analysis of RNA Modifications by Second-and Third-Generation Deep Sequencing: 2020 Update. (2021) doi:10.3390/genes12020278.

156. Flynn, R. A. *et al.* Small RNAs are modified with N-glycans and displayed on the surface of living cells. *Cell* **184**, 3109-3124.e22 (2021).

157. Wetzel, C. & Limbach, P. A. Mass spectrometry of modified RNAs: recent developments. *Analyst* **141**, 16–23 (2016).

158. Taucher, M. & Breuker, K. Top-Down Mass Spectrometry for Sequencing of Larger (up to 61 nt) RNA by CAD and EDD. *J Am Soc Mass Spectrom* **21**, 918–929 (2010).

159. Peters-Clarke, T. M. *et al.* Ribonucleic acid sequence characterization by negative electron transfer dissociation mass spectrometry. *Anal Chem* **92**, 4436 (2020).

160. Calderisi, G., Glasner, H. & Breuker, K. Radical Transfer Dissociation for De Novo Characterization of Modified Ribonucleic Acids by Mass Spectrometry. *Angewandte Chemie (International Ed. in English)* **59**, 4309 (2020).

161. Huang, T. Y., Liu, J. & McLuckey, S. A. Top-Down Tandem Mass Spectrometry of tRNA Via Ion Trap Collision-Induced Dissociation. *J Am Soc Mass Spectrom* **21**, 890–898 (2010).

162. Schneeberger, E.-M., Breuker, K., Schneeberger, E.-M. & Breuker, Riv.-D. K. Native Top-Down Mass Spectrometry of TAR RNA in Complexes with a Wild-Type tat Peptide for Binding Site Mapping. *Angewandte Chemie International Edition* **56**, 1254–1258 (2017).

163. Schneeberger, E. M. *et al.* Native mass spectrometry reveals the initial binding events of HIV-1 rev to RRE stem II RNA. *Nature Communications 2020 11:1* **11**, 1–10 (2020).

164. Hagelskamp, F. *et al.* Broadly applicable oligonucleotide mass spectrometry for the analysis of RNA writers and erasers in vitro. *Nucleic Acids Research* **48**, e41–e41 (2020).

165. Wetzel, C. & Limbach, P. A. Mass spectrometry of modified RNAs: recent developments. *Analyst* **141**, 16–23 (2015).

166. Ross, R. L., Cao, X. & Limbach, P. A. Mapping Post-Transcriptional Modifications onto Transfer Ribonucleic Acid Sequences by Liquid Chromatography Tandem Mass Spectrometry. (2017) doi:10.3390/biom7010021.

167. Yoluç, Y. *et al.* Instrumental analysis of RNA modifications. *https://doi.org/10.1080/10409238.2021.1887807* **56**, 178–204 (2021).

168. Nyakas, A., Eberle, R. P., Stucki, S. R. & Schürch, S. More than charged base loss--revisiting the fragmentation of highly charged oligonucleotides. *J Am Soc Mass Spectrom* **25**, 1155–1166 (2014).

169. Nyakas, A., Stucki, S. R. & Schürch, S. Tandem mass spectrometry of modified and platinated oligoribonucleotides. *J Am Soc Mass Spectrom* **22**, 875–887 (2011).

170. Huang, T. yi, Kharlamova, A., Liu, J. & McLuckey, S. A. Ion trap collision-induced dissociation of multiply deprotonated RNA: c/y-ions versus (a-B)/w-ions. *J Am Soc Mass Spectrom* **19**, 1832–1840 (2008).

171. Rozenski, J. & McCloskey, J. A. SOS: a simple interactive program for ab initio oligonucleotide sequencing by mass spectrometry. *J Am Soc Mass Spectrom* **13**, 200–203 (2002).

172. Matthiesen, R. & Kirpekar, F. Identification of RNA molecules by specific enzyme digestion and mass spectrometry: software for and implementation of RNA mass mapping. *Nucleic Acids Res* **37**, (2009).

173. Nakayama, H. *et al.* Ariadne: a database search engine for identification and chemical analysis of RNA using tandem mass spectrometry data. *Nucleic Acids Res* **37**, (2009).

174. Nyakas, A., Blum, L. C., Stucki, S. R., Reymond, J. L. & Schürch, S. OMA and OPA--software-supported mass spectra analysis of native and modified nucleic acids. *J Am Soc Mass Spectrom* **24**, 249–256 (2013).

175. Sample, P. J., Gaston, K. W., Alfonzo, J. D. & Limbach, P. A. RoboOligo: software for mass spectrometry data to support manual and de novo sequencing of post-transcriptionally modified ribonucleic acids. *Nucleic Acids Res* **43**, (2015).

176. Paulines, M. J., Wetzel, C. & Limbach, P. A. Using spectral matching to interpret LC-MS/MS data during RNA modification mapping. *J Mass Spectrom* **54**, 906–914 (2019).

177. Lobue, P. A., Yu, N., Jora, M., Abernathy, S. & Limbach, P. A. Improved application of RNAModMapper - An RNA modification mapping software tool - For analysis of liquid chromatography tandem mass spectrometry (LC-MS/MS) data. *Methods* **156**, 128–138 (2019).

178. Wein, S. *et al.* A computational platform for high-throughput analysis of RNA sequences and modifications by mass spectrometry. *Nat Commun* **11**, (2020).

179. Limbach, P. A., Crain, P. F. & McCloskey, J. A. Summary: the modified nucleosides of RNA. *Nucleic Acids Res* **22**, 2183–2196 (1994).

180. Sarin, L. P. *et al.* Nano LC-MS using capillary columns enables accurate quantification of modified ribonucleosides at low femtomol levels. *RNA* **24**, rna.065482.117 (2018).

181. Borland, K. *et al.* Production and Application of Stable Isotope-Labeled Internal Standards for RNA Modification Analysis. *Genes 2019, Vol. 10, Page 26* **10**, 26 (2019).

182. Kellner, S. *et al.* Absolute and relative quantification of RNA modifications via biosynthetic isotopomers. *Nucleic Acids Res* **42**, (2014).

183. Zhao, W. *et al.* Comparison of RNA-Seq by poly (A) capture, ribosomal RNA depletion, and DNA microarray for expression profiling. *BMC Genomics* **15**, 1–11 (2014).

184. Sultan, M. *et al.* Influence of RNA extraction methods and library selection schemes on RNA-seq data. *BMC Genomics* **15**, 1–13 (2014).

185. Legrand, C. *et al.* Statistically robust methylation calling for whole-transcriptome bisulfite sequencing reveals distinct methylation patterns for mouse RNAs. (2017) doi:10.1101/gr.210666.116.

186. Delaunay, S. & Frye, M. RNA modifications regulating cell fate in cancer. *Nature Cell Biology* **21**, 552–559 (2019).

187. Barbieri, I. & Kouzarides, T. Role of RNA modifications in cancer. *Nature Reviews Cancer* vol. 20 303–322 (2020).

188. Haruehanroengra, P., Zheng, Y. Y., Zhou, Y., Huang, Y. & Sheng, J. RNA modifications and cancer. *https://doi.org/10.1080/15476286.2020.1722449* **17**, 1560–1575 (2020).

189. Kim, Y. K., Yeo, J., Kim, B., Ha, M. & Kim, V. N. Short structured RNAs with low GC content are selectively lost during extraction from a small number of cells. *Mol Cell* **46**, 893–895 (2012).

190. Brawerman, G., Mendecki, J. & Lee, S. Y. A procedure for the isolation of mammalian messenger ribonucleic acid. *Biochemistry* **11**, 637–641 (1972).

191. Cai, W. M. *et al.* A platform for discovery and quantification of modified ribonucleosides in RNA: Application to stress-induced reprogramming of tRNA modifications. *Methods Enzymol* **560**, 29 (2015).

192. Zhang, L. S. *et al.* Transcriptome-wide Mapping of Internal N 7-Methylguanosine Methylome in Mammalian mRNA. *Mol Cell* **74**, 1304-1316.e8 (2019).

193. Matuszewski, M. *et al.* A hydantoin isoform of cyclic N6-threonylcarbamoyladenosine (ct6A) is present in tRNAs. *Nucleic Acids Res* **45**, 2137–2149 (2017).

194. Jora, M. *et al.* Chemical Amination/Imination of Carbonothiolated Nucleosides During RNA Hydrolysis. *Angewandte Chemie International Edition* **60**, 3961–3966 (2021).

195. Taniguchi, T. *et al.* Decoding system for the AUA codon by tRNAIle with the UAU anticodon in Mycoplasma mobile. *Nucleic Acids Res* **41**, 2621–2631 (2013).

196. Wakimoto, H. *et al.* Human glioblastoma-derived cancer stem cells: Establishment of invasive glioma models and treatment with oncolytic herpes simplex virus vectors. *Cancer Research* **69**, 3472–3481 (2009).

197. Wakimoto, H. *et al.* Maintenance of primary tumor phenotype and genotype in glioblastoma stem cells. *Neuro-Oncology* **14**, 132–144 (2012).

198. Su, D. *et al.* Quantitative analysis of ribonucleoside modifications in tRNA by HPLC-coupled mass spectrometry. *Nature Protocols* **9**, 828–841 (2014).

199. Esteller, M. & Pandolfi, P. P. The Epitranscriptome of Noncoding RNAs in Cancer. *Cancer Discovery* **7**, 359 LP – 368 (2017).

200. Basanta-Sanchez, M., Temple, S., Ansari, S. A., D'Amico, A. & Agris, P. F. Attomole quantification and global profile of RNA modifications: Epitranscriptome of human neural stem cells. *Nucleic Acids Research* **44**, 1–10 (2016).

201. Rose, R. E., Pazos, M. A., Curcio, M. J. & Fabris, D. Global Epitranscriptomics Profiling of RNA Post-Transcriptional Modifications as an Effective Tool for Investigating the

Epitranscriptomics of Stress Response. *Molecular & Cellular Proteomics* **15**, 932–944 (2016).

202. Yoluç, Y., van de Logt, E. & Kellner-Kaiser, S. The Stress-Dependent Dynamics of Saccharomyces cerevisiae tRNA and rRNA Modification Profiles. (2021) doi:10.3390/genes12091344.

203. Wang, H. *et al.* Epitranscriptomic profile of Lactobacillus agilis and its adaptation to growth on inulin. doi:10.1186/s13104-021-05563-2.

204. Chan, C., Pham, P., Dedon, P. C. & Begley, T. J. Lifestyle modifications: Coordinating the tRNA epitranscriptome with codon bias to adapt translation during stress responses. *Genome Biology* **19**, 1–11 (2018).

205. Ng, C. S. *et al.* tRNA epitranscriptomics and biased codon are linked to proteome expression in Plasmodium falciparum. *Molecular Systems Biology* **14**, e8009 (2018).

206. Hammam, E. *et al.* Malaria Parasite Stress Tolerance Is Regulated by DNMT2- Mediated tRNA Cytosine Methylation. *mBio* **12**, (2021).

207. Liu, P. *et al.* Preclinical models of glioblastoma: limitations of current models and the promise of new developments. *Expert Reviews in Molecular Medicine* **23**, (2021).

208. Crystal, A. S. *et al.* Patient-derived models of acquired resistance can identify effective drug combinations for cancer. *Science* **346**, 1480–1486 (2014).

209. da Hora, C. C., Schweiger, M. W., Wurdinger, T. & Tannous, B. A. Patient-Derived Glioma Models: From Patients to Dish to Animals. *Cells 2019, Vol. 8, Page 1177* **8**, 1177 (2019).

210. Kodack, D. P. *et al.* Primary Patient-Derived Cancer Cells and Their Potential for Personalized Cancer Patient Care. *Cell Reports* **21**, 3298 (2017).

211. Chong, J., Wishart, D. S. & Xia, J. Using MetaboAnalyst 4.0 for Comprehensive and Integrative Metabolomics Data Analysis. *Current Protocols in Bioinformatics* **68**, e86 (2019).

212. Dominissini, D. *et al.* Topology of the human and mouse m6A RNA methylomes revealed by m6A-seq. *Nature* **485**, 201–206 (2012).

213. Jia, G. *et al.* N6-Methyladenosine in nuclear RNA is a major substrate of the obesity-associated FTO. *Nature Chemical Biology* **7**, 885–887 (2011).

214. Agris, P. F. The importance of being modified: an unrealized code to RNA structure and function. *Rna* **21**, 552–554 (2015).

215. Dong, Z. & Cui, H. The Emerging Roles of RNA Modifications in Glioblastoma. *Cancers (Basel)* **12**, 736 (2020).

216. Wang, P. *et al.* Identification of RNA: 5-Methylcytosine Methyltransferases-Related Signature for Predicting Prognosis in Glioma. *Frontiers in Oncology* **10**, (2020).

217. Helm, M., Lyko, F. & Motorin, Y. Limited antibody specificity compromises epitranscriptomic analyses. *Nature Communications* vol. 10 (2019).

218. Novoa, Eva Maria, Mason, christopher & Mattick, J. S. Charting the unknown epitranscriptome. *Nature Reviews Molecular Cell Biology* **18**, 339–340 (2017).

219. Cech, N. B. & Enke, C. G. Practical implications of some recent studies in electrospray ionization fundamentals. *Mass Spectrometry Reviews* **20**, 362–387 (2001).

220. Brennan, C. W. *et al.* The Somatic Genomic Landscape of Glioblastoma. *Cell* **155**, 462–477 (2013).

221. Parker, N. R., Khong, P., Parkinson, J. F., Howell, V. M. & Wheeler, H. R. Molecular heterogeneity in glioblastoma: Potential clinical implications. *Frontiers in Oncology* **5**, 55 (2015).

222. Iser, I. C., Pereira, M. B., Lenz, G. & Wink, M. R. The Epithelial-to-Mesenchymal Transition-Like Process in Glioblastoma: An Updated Systematic Review and In Silico Investigation. *Medicinal Research Reviews* **37**, 271–313 (2016).

223. Dirkse, A. *et al.* Stem cell-associated heterogeneity in Glioblastoma results from intrinsic tumor plasticity shaped by the microenvironment. *Nature Communications 2019 10:1* **10**, 1–16 (2019).

224. Wang, L. *et al.* The Phenotypes of Proliferating Glioblastoma Cells Reside on a Single Axis of Variation. *Cancer Discov* **9**, 1708–1719 (2019).

225. Marziali, G. *et al.* Metabolic/Proteomic Signature Defines Two Glioblastoma Subtypes With Different Clinical Outcome. *Sci Rep* **6**, (2016).

226. Teng, J. *et al.* Dissecting inherent intratumor heterogeneity in patient-derived glioblastoma culture models. *Neuro-Oncology* **19**, 820–832 (2017).

227. Hiddingh, L. *et al.* EFEMP1 induces γ-secretase/Notch-mediated temozolomide resistance in glioblastoma. *Oncotarget* **5**, 363 (2014).

228. Xia, J., Psychogios, N., Young, N. & Wishart, D. S. MetaboAnalyst: a web server for metabolomic data analysis and interpretation. *Nucleic Acids Research* **37**, W652–W660 (2009).

229. Wiener, D. & Schwartz, S. The epitranscriptome beyond m 6 A. *Nat Rev Genet* **22**, 119–131 (2021).

230. Kimura, S. *et al.* Discovery of the β-barrel–type RNA methyltransferase responsible for N6-methylation of N6-threonylcarbamoyladenosine in tRNAs. *Nucleic Acids Research* **42**, 9350–9365 (2014).

231. Edvardson, S. *et al.* tRNA N6-adenosine threonylcarbamoyltransferase defect due to KAE1/TCS3 (OSGEP) mutation manifest by neurodegeneration and renal tubulopathy. *European Journal of Human Genetics* **25**, 545–551 (2017).

232. Heissenberger, C. *et al.* Loss of the ribosomal RNA methyltransferase NSUN5 impairs global protein synthesis and normal growth. *Nucleic Acids Research* **47**, 11807–11825 (2019).

233. Agris, P. F., Vendeix, F. A. P. & Graham, W. D. tRNA's Wobble Decoding of the Genome: 40 Years of Modification. *Journal of Molecular Biology* vol. 366 1–13 (2007).

234. Seelam Prabhakar, P., Takyi, N. A. & Wetmore, S. D. Post-transcriptional modifications at the 37 th position in the anticodon stem loop of tRNA: Structural insights from MD simulations.

235. Berdasco, M. & Esteller, M. Towards a druggable epitranscriptome: Compounds that target RNA modifications in cancer. *British Journal of Pharmacology* **179**, 2868–2889 (2022).